Synthesis, Structure, and Properties of an Undecairon(III) Oxo-Hydroxo Aggregate: An Approach to the Polyiron Core in Ferritin

Sergiu M. Gorun,[1a] Georgia C. Papaefthymiou,[1b] Richard B. Frankel,[1b] and Stephen J. Lippard*[1a]

Contribution from the Department of Chemistry and the Francis Bitter National Magnet Laboratory, Massachusetts Institute of Technology, Cambridge, Massachusetts 02139.
Received November 11, 1986

Abstract: A novel, discrete undecairon(III) oxo-hydroxo aggregate, $[Fe_{11}O_6(OH)_6(O_2CPh)_{15}]$, has been synthesized by controlled hydrolytic polymerization in nonaqueous solvents of simple mononuclear and oxo-bridged binuclear ferric salts. The complex was structurally characterized in two crystalline forms. In the rhombohedral form, $[Fe_{11}O_6(OH)_6(O_2CPh)_{15}]\cdot 6THF$, the molecules have crystallographically required D_3 symmetry. The eleven iron atoms define a twisted, pentacapped trigonal prism. Two type A iron atoms located on the threefold symmetry axis are joined by μ_3-oxo bridges to six type B iron atoms at the corners of the twisted trigonal prism. These type B iron atoms are linked to one another and to three type C iron atoms, situated on twofold symmetry axes, by μ_3-hydroxo bridges. A sheath of 15 bidentate bridging benzoate ligands, no two of which join the same pair of iron atoms, completes the pseudooctahedral coordination about each of the 11 high spin ferric centers. The Fe-O bond lengths range from 1.876 (5) Å for Fe-(μ-oxo) to 2.106 (8) Å for Fe-O(benzoate) type interactions. The six tetrahydrofuran molecules penetrate the sheath of benzoate ligands to form hydrogen bonds to protons on the six μ_3-hydroxo ligands. The other crystalline form, $[Fe_{11}O_6(OH)_6(O_2CPh)_{15}]\cdot H_2O\cdot 8MeCN$, is triclinic and has no imposed molecular site symmetry. The molecular geometry of the undecairon(III) aggregate, however, is nearly identical with that in the rhombohedral form. Solutions of $[Fe_{11}O_6(OH)_6(O_2CPh)_{15}]$ in dry CH_2Cl_2 or CH_3CN are indefinitely stable, judging by optical spectroscopy. Cyclic voltammetric studies in the former solvent revealed a quasi-reversible one-electron reduction at $E_{1/2} = -0.309$ V vs. SCE, tentatively assigned to the formation of $[Fe_{11}O_6(OH)_6(O_2CPh)_{15}]^-$, as well as two irreversible waves with peak currents at -0.817 and -1.323 V. The temperature-dependent magnetic susceptibility behavior of the undecairon(III) aggregate is consistent with a ground state spin $S_T = {}^1/_2$ per aggregate and internal antiferromagnetic coupling. High-field magnetization and Mössbauer experiments reveal that the individual Fe_{11} molecules have incipient magnetic order with very low anisotropy and some exchange interactions on the order of 10 cm^{-1}. The presence of μ_3-oxo, μ_3-hydroxo, and carboxylate ligands, as well as the manner in which $[Fe_{11}O_6(OH)_6(O_2CPh)_{15}]$ self-assembles, make it an attractive model for the polyiron core in ferritin. Comparisons of the structural, magnetic, and spectroscopic properties of the two systems are discussed.

Iron is an important element in inorganic chemistry, mineralogy, and biology. The hydrolytic polymerization of iron, which has been extensively studied,[2] is involved in the formation of iron-containing minerals and in iron deposition during biomineralization[3] of magnetotactic organisms and iron storage proteins.[4,5]

In mammals, iron is stored in ferritin, a protein that sequesters iron(III) as a polymeric oxo-hydroxo complex.[6] The three-dimensional structure of apoferritin is comprised of 24 cylindrical subunits which form a rhombic dodecahedron with 432 point symmetry. In the center there is a cavity shielded from the external aqueous environment by the hydrophobic surfaces of the subunits. Connecting the cavity with the protein exterior are six hydrophobic (4-fold symmetry) and eight hydrophilic (3-fold symmetry) channels. Hydrophobicity is conveyed by 12 leucine residues which line each 4-fold channel, while hydrophilicity is conferred by three aspartate and three glutamate residues lining each of the funnel-shaped 3-fold channels. The interior of the cavity is coated with hydrophilic residues (carboxylates, amino groups, and imidazoles) which are crystallographically disordered in the absence of metal ions. Approximately 1200 iron atoms are usually stored in the cavity, although it can accommodate up to 4500. The internal and external diameters of the protein shell are 70-80 and 125-135 Å, respectively.

The nucleation process for iron storage in ferritin may start in the cavity or at the hydrophilic channel-cavity interface and may involve a mixed-valence, oxo-bridged, binuclear Fe(II)-Fe(III) complex.[7,8] The exterior hydrophilicity of the protein sheath ensures its solubility in vivo and the interior hydrophilicity provides optimum binding properties for the metal core; the intervening hydrophobic region both separates and links the two. The core formation and the iron-releasing mechanisms are not yet established; however, available evidence[6] is consistent with the following structural or mechanistic features: (i) Apoprotein is formed before iron is deposited in the core. (ii) Iron enters the apoferritin shell as Fe(II) and is oxidized in the presence of O_2, either in the channels or at the interior interface, with the formation of a (number of) small "initiation" complex(es). (iii) Subsequent addition of Fe(II) ions leads to the growth of a crystallite through hydrolytic polymerization, probably accompanied by oxidation to Fe(III) at the surface of the metallic core. (iv) Carboxylic acid residues are the major binding sites for iron and are essential for its incorporation. (v) Iron is released upon reduction and/or chelation by ligands which may or may not penetrate through the hydrophobic channels to the core.

(1) (a) Department of Chemistry. (b) Francis Bitter National Magnet Laboratory.
(2) Flynn, C. M., Jr. *Chem. Rev.* **1986**, *84*, 31-41.
(3) Lowenstam, H. A. *Science* **1981**, *211*, 1126-1130.
(4) Towe, K. M.; Lowenstam, H. A.; Nesson, M. H. *Science* **1963**, *142*, 63-64.
(5) Mann, S.; Frankel, R. B.; Blakemore, R. P. *Nature (London)* **1984**, *310*, 405-407.
(6) (a) Ford, G. C.; Harrison, P. M.; Rice, D. W.; Smith, J. M. A.; Treffry, A.; White, J. L.; Yariv, J. *Phil. Trans. R. Soc. London B* **1984**, *304*, 551-565. (b) Ford, G. C.; Harrison, P. M.; Rice, D. W.; Smith, J. M. A.; Treffry, A.; White, J. L.; Yariv, J. *Rev. Port. Quim.* **1985**, *27*, 119-120. (c) Spiro, T. G.; Saltman, P. *Struct. Bond.* **1969**, *6*, 116-156. (d) Spiro, T. G.; Pope, L.; Saltman, P. *J. Am. Chem. Soc.* **1967**, *89*, 5555-5559. (e) Spiro, T. G.; Bates, G.; Saltman, P. *J. Am. Chem. Soc.* **1967**, *89*, 5559-5562. (f) Theil, E. C. *Adv. Inorg. Biochem.* **1983**, *5*, 1-38 and references cited therein. (g) Fischbach, F. A.; Anderegg, J. W. *J. Mol. Biol.* **1965**, *14*, 458-473. (h) Smith, J. M. A.; Helliwell, J. R. *Inorg. Chim. Acta* **1985**, *106*, 193-196. (i) Mann, S.; Bannister, J. V.; Williams, R. J. P. *J. Mol. Biol.* **1986**, *188*, 225-232.
(7) (a) Chasteen, N. D.; Antanaitis, B. C.; Aisen, P. *J. Biol. Chem.* **1985**, *260*, 2926-2929. (b) Crichton, R. R. *Struct. Bond. (Berlin)* **1973**, *17*, 67-134. (c) *Proteins of Iron Storage and Transport in Biochemistry and Medicine*, Crichton, R. R., Ed., North Holland: Amsterdam, 1975.
(8) Chasteen, N. D.; Theil, E. C. *J. Biol. Chem.* **1982**, *257*, 7672-7677.

0002-7863/87/1509-3337$01.50/0 © 1987 American Chemical Society

The molecular formula of the horse spleen ferritin core is approximately $\{[FeO(OH)]_8[FeO(O_2PO_2H_2)]\}_n$ and its structure has been compared with that of the mineral ferrihydrite, $5Fe_2O_3 \cdot 9H_2O$.[9] This evidence, along with in vitro reconstitution experiments, indicates that about 60–80% of the phosphate in ferritin is adventitious. A recent determination[6i] of the Fe and P content of thalassemic human ferritin cores indicates an Fe/P atomic ratio of 21.0. The structure of ferrihydrite consists of FeO_6 octahedra arranged three dimensionally with underpopulated iron sites, comparable to α-hematite (Fe_2O_3), with O^{2-} anions being replaced by H_2O, OH^-, or a combination of both.

The preparation of models for the ferritin core has been a challenge to synthetic inorganic chemists. In *aqueous solutions* mixtures of polymers have been obtained[10,11] when Fe(III) salts are hydrolyzed, but reliable structural information is lacking. An octanuclear iron complex containing 1,4,7-triazacyclononane (TACN) ligands, $[Fe_8O_2(OH)_{12}(TACN)_6]^{8+}$,[12] was isolated and several planar tetranuclear cores of the type $\{Fe_4(\mu_3\text{-}O)_2\}^{8+}$ [13] or $\{Fe_4(\mu_3\text{-}OH)_2\}^{10+}$ [14] are known to occur in nature. A tetrahedral $\{Fe_4(\mu_2\text{-}O)_2(\mu_2\text{-}OH)_2(\mu_2\text{-}OR)_2\}^{4+}$ species has also been recently reported.[15] On the other hand, in *nonaqueous solvents* we have obtained $\{Fe_3O\}^{7+}$ and $\{Fe_4O_2\}^{8+}$ units from mononuclear $[FeCl_4]^-$ and $[Fe_2OCl_6]^{2-}$ building blocks[16–18] in the presence of ligands containing carboxylate and polypyrazolyl or -imidazolyl coordinating moieties. The ability of oxo-bridged diiron(III) units to aggregate in this manner (eq 1 and 2) prompted us to attempt the synthesis of even larger oxo-bridged polyiron(III) aggregates

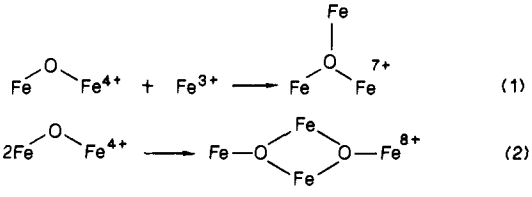

approximating the ferritin core, in the absence of nitrogen donor ligands. As described in preliminary form,[19] this approach led to the discovery of a remarkable molecule, $[Fe_{11}O_6(OH)_6(O_2CPh)_{15}]$, the synthesis and properties of which form the focus of the present full report.

Experimental Section

Materials and Methods. Preparation of Compounds. Solvents and reagents were obtained from commercial sources and used without further purification unless otherwise stated. Tetrahydrofuran (THF), acetonitrile (MeCN), and methylene chloride were dried by distillation from potassium/benzophenone, calcium hydride, and P_2O_5, respectively. $(Et_4N)[FeCl_4]$ was prepared from Et_4NCl and $FeCl_3 \cdot 6H_2O$ by a method similar to that employed for the iron(II) analogue.[20] $(Et_4N)_2[Fe_2OCl_6]$ was prepared by a literature procedure.[21] Elemental analyses were performed by Atlantic Microlab, Inc., Atlanta, GA, Galbraith Laboratories, Knoxville, TN, and Spang Microanalytical Laboratory, Eagle Harbor, MI.

$[Fe_{11}O_6(OH)_6(O_2CPh)_{15}] \cdot H_2O \cdot 8MeCN$ ($1 \cdot H_2O \cdot 8MeCN$). To a clear solution containing 0.351 g (5.8×10^{-4} mol) of $(Et_4N)_2[Fe_2OCl_6]$ in 6 mL of MeCN were added 0.169 g (11.7×10^{-4} mol) of anhydrous sodium benzoate with rapid stirring. After 1 h the solution was filtered and water vapor was allowed to diffuse into it. Two weeks later, red-brown crystals were isolated and shown by X-ray diffraction (vide infra) to contain the undecairon complex $[Fe_{11}O_6(OH)_6(O_2CPh)_{15}]$ (**1**). Analytical data were consistent with one water and two acetonitrile molecules of crystallization (but see discussion of X-ray results below). Anal. Calcd for $Fe_{11}C_{109}H_{89}O_{43}N_2$ ($1 \cdot H_2O \cdot 2MeCN$): C, 47.97; H, 3.29. Found: C, 48.08; H, 3.30. A check for chlorine gave zero or trace amounts. IR (KBr, cm^{-1}) 3601, 3065, 1701, 1597, 1557, 1413, 1308, 1177, 1157, 1070, 1026, 841, 809, 718, 688, 677, 642, 477.

$[Fe_{11}O_6(OH)_6(O_2CPh)_{15}] \cdot 6THF$ ($1 \cdot 6THF$). Method A. To a clear solution containing 9.43 g (1.57×10^{-2} mol) of $(Et_4N)_2[Fe_2OCl_6]$ in 163 mL of MeCN were added 4.533 g (3.14×10^{-2} mol) of anhydrous sodium benzoate with vigorous stirring. The suspension was filtered after 22 h and the filtrate was layered over an equal volume of a solution of 0.8% H_2O in THF. After 4 weeks, red-brown crystals were isolated as follows. The crude material, which contained a small amount of a flocculent precipitate, was decanted and the solid was stirred with a 10:1 (v/v) THF:MeCN mixture. After the majority of the crystals settled, the suspension was again decanted, and the procedure was repeated a few more times. The yield was 57%, based on sodium benzoate (limiting reagent). The crystals lost solvent readily and were dried in vacuo prior to analysis. Anal. Calcd for $Fe_{11}C_{105}H_{81}O_{42}$: C, 47.97; H, 3.11; Fe, 23.37; O, 25.55. Found: C, 47.95; H, 3.16; Fe, 23.14; O, 25.75 by difference. IR (KBr, cm^{-1}) (see above). UV–vis (CH_2Cl_2), λ (ϵ per iron, $M^{-1}\,cm^{-1}$) 232 (1.63×10^4), 273 (sh), 304 (sh), 492 (sh, 132), 881 (~6) nm.

Method B. To a clear solution containing 0.2 g (3.33×10^{-4} mol) of $(Et_4N)_2[Fe_2OCl_6]$ in 10 mL of MeCN were added 0.11 g (3.35×10^{-4} mol) of $(Et_4N)[FeCl_4]$ with vigorous stirring. After 1 h, 0.15 g (10.4×10^{-4} mol) of anhydrous sodium benzoate were added and stirring was continued for 2 h. The suspension was filtered, and the procedure described in Method A was followed to obtain pure crystals. Method B was generally employed to obtain **1** after the structures of both crystalline modifications were known.

Collection and Reduction of X-ray Data. Beautiful red polyhedral crystals of $1 \cdot H_2O \cdot 8MeCN$ and $1 \cdot 6THF$ were mounted in 0.7 mm diameter glass capillaries with mother liquor to avoid solvent loss. Both crystal forms lose solvent readily. In both cases, data sets were collected at room temperature and no decay in the intensity of standard reflections was noticed. Owing to the fairly regular shape of the crystals and the low value of their linear absorption coefficients, no absorption corrections were applied. Study on the diffractometer indicated that $1 \cdot H_2O \cdot 8MeCN$ belongs to the triclinic system. The choice of the space group $P\bar{1}$ (C_i^1, No. 2)[22a] was confirmed by statistical analysis of data[23] and by the successful solution and refinement of the structure. Data collection and reduction were carried out as previously described,[24] details of which are provided in Table I.

Intensity data collected for $1 \cdot 6THF$ were based on a preliminary unit cell determination indicating a C-centered monoclinic space group. Since a glide plane was not found, the possible space groups were $C2$ (C_2^3, No. 5),[22b] Cm (C_s^3, No. 8),[22c] and $C2/m$ (C_{2h}^3, No. 12).[22d] A statistical Debye–Wilson plot suggested an acentric space group, tentatively excluding $C2/m$ from the above list. A solution was found only in $C2$ (see below). The final metric parameters of the unit cell were employed in a systematic check for higher symmetry by using the program TRACER[25] which indicated that the crystal actually belongs to the trigonal (rhombohedral)

(9) Chukrov, F. V.; Zvyagin, B. B.; Gorschkov, A. I.; Yermilova, L. P.; Balashova, V. V. **1973**, *Izv. Akad. Nauk. SSSR, Ser. Geol.* **1973**, 23–33; *Int. Geol. Rev. 16*, 1131–1143.
(10) (a) Spiro, T. G.; Allerton, S. E.; Denner, J.; Terzis, A.; Bils, R.; Saltman, P. *J. Am. Chem. Soc.* **1966**, *88*, 2721–2726. (b) Brady, G. W.; Kurkjian, C. R.; Lyden, E. F. X.; Robin, M. B.; Saltman, P.; Spiro, T.; Tersis, A. *Biochemistry* **1968**, *7*, 2185–2192.
(11) (a) Sommer, B. A.; Margerum, D. W.; Reuner, J.; Saltman, P.; Spiro, T. G. *Bioinorg. Chem.* **1973**, *2*, 295–309. (b) Catterick, J.; Thornton, P. *J. Chem. Soc., Dalton Trans.* **1977**, 1420–1425.
(12) Wieghardt, K.; Pohl, K.; Jibril, I.; Huttner, G. *Angew. Chem., Intl. Ed. Engl.* **1984**, *23*, 77–78.
(13) (a) Susse, P. *Z. Kristallogr.* **1968**, *127*, 261–275. (b) Ponomarev, V. I.; Atovmyan, L. O.; Bobkova, S. A.; Turtē, K. I. *Dokl. Akad. Nauk. SSSR* **1984**, *274*, 368–372.
(14) Moore, P. B. *Ann. Mineral.* **1972**, *57*, 397–410.
(15) Murch, B. P.; Boyle, P. D.; Que, L. *J. Am. Chem. Soc.* **1985**, *107*, 6728–6729.
(16) (a) Gorun, S. M.; Lippard, S. J. *J. Am. Chem. Soc.* **1985**, *107*, 4568–4570. (b) Gorun, S. M.; Papaefthymiou, G. C.; Frankel, R. B.; Lippard, S. J. *J. Am. Chem. Soc.*, in press.
(17) (a) Gorun, S. M. Ph.D. Thesis, Massachusetts Institute of Technology, 1986. (b) Gorun, S. M.; Lippard, S. J., to be submitted for publication.
(18) Armstrong, W. H.; Roth, M. E.; Lippard, S. J., submitted for publication.
(19) Gorun, S. M.; Lippard, S. J. *Nature (London)* **1986**, *319*, 666–668.
(20) Gill, N. S.; Taylor, F. B. *Inorg. Synth.* **1967**, *9*, 136–142.
(21) Armstrong, W. H.; Lippard, S. J. *Inorg. Chem.* **1985**, *24*, 981–982.
(22) *International Tables for Crystallography*; Hahn, T., Ed.; D. Reidel Publishing Co., Dordrecht: Holland/Boston, USA, 1983; Volume A: (a) p 104, (b) p 114, (c) p 134, (d) p 158, (e) p 506.
(23) Germain, G.; Main, P.; Woolfson, M. M. *Acta Crystallogr., Sect. A* **1971**, *A27*, 368–376.
(24) Silverman, L. D.; Dewan, J. C.; Giandomenico, C. M.; Lippard, S. J. *Inorg. Chem.* **1980**, *19*, 3379–3383 and references cited therein.
(25) Lawton, S. L. *TRACER II, A FORTRAN Lattice Transformation-Cell Reduction Program*; Mobil Oil Corporation, Paulsboro, NJ, 1967.
(26) Structure factor calculations and least squares refinement were carried out with SHELX-76: Sheldrick, G. M. In *Computing in Crystallography*; Schenk, H., Olthoff-Hazekamp, R., Van Koningsveld, H., Bassi, G. C., Eds.; Delft University Press: Delft, The Netherlands, 1978; pp 34–42. We thank G. M. Sheldrick for kindly providing a version of SHELX-76, extended by D. Rabinowich and K. Reich to handle 400 atoms and 500 parameters.

Table I. Experimental Details of the X-ray Crystallographic Studies of $[Fe_{11}O_6(OH)_6(O_2CPh)_{15}]$ (**1**), as **1**·H_2O·8MeCN and **1**·6THF

(A) Crystal Parameters[a]

	1·H_2O·8MeCN	**1**·6THF		**1**·H_2O·8MeCN	**1**·6THF
a, Å	19.518 (2)	18.521 (3)	space group	$P\bar{1}$	R32
b, Å	22.696 (3)				
c, Å	16.485 (2)	46.659 (6)	*Z*	2	3
α, deg	94.60 (1)	90.0			
β, deg	93.47 (1)	90.0	ρ_{calcd} (g/cm^3)	1.371	1.100
γ, deg	81.61 (1)	120.0	mol wt	2975.5	3061.7
vol, Å^3	7209	13855			

(B) Measurement and Treatment of Intensity Data[b]

Instrument: Enraf-Nonius CAD-4F κ-geometry diffractometer
radiation: Mo Kα (λ_α = 0.71073 Å) graphite monochromatized

	1·H_2O·8MeCN	**1**·6THF
no. of reflcns collected	23601	5969
no. of unique reflcns	10205	3223
range of 2θ, deg	$3 \leq 2\theta \leq 47$	$3 \leq 2\theta \leq 41$
standards	(1,6,5), ($\bar{1}$,10,$\bar{5}$), (1,6,$\bar{6}$)	(1,9,$\bar{2}$), (1,5,$\bar{6}$), (2,10,$\bar{1}$)
R_{av}[b]	0.025	0.012
monitoring interval	3600 s	3600 s
linear abs coeff, cm^{-1}	10.9	8.45
low angle ω scans, $\Delta\omega_{1/2}$, deg	0.20	0.23

(C) Final Least-Squares Refinement Results

	1·H_2O·8MeCN	**1**·6THF
R_1[c]	0.098	0.051
R_2[c]	0.111	0.077
no. of unique obsd reflcns	9506	2643
threshold	$F_o > 6\sigma(F_o)$	$F_o > 6\sigma(F_o)$
no. of parameters	868	265

[a] From a least-squares fit to the setting angles of 25 reflections with $2\theta \geq 30°$ for **1**·H_2O·8MeCN and $2\theta \geq 20°$ for **1**·6THF. [b] See ref 24. [c] $R_1 = \sum||F_o| - |F_c||/\sum|F_o|$; $R_2 = [\sum w(|F_o| - |F_c|)^2/\sum wF_o^2]^{1/2}$.

system. Transformation of the monoclinic space group *C*2 to the trigonal system by using the matrix (0.5, 0.5, 0; 0.5, 0.5, 0; −1, 0, −3) gave space group *R*32 (D_3^7, No. 155).[22e] The choice of rhombohedral symmetry was confirmed by the low value for R_{av} (Table I) obtained upon averaging equivalent reflections in the higher symmetry cell. Moreover, reflections expected to be systematically absent in *R*32 were not observed in *C*2 and the structure was successfully refined in the higher symmetry space group. Additional details may be found in Table I.

Structure Solution and Refinement. $[Fe_{11}O_6(OH)_6(O_2CPh)_{15}]$·$H_2O$·8MeCN (1·$H_2O$·8MeCN). Atomic coordinates of the eleven iron atoms were determined by direct methods with MULTAN.[23] Subsequent difference Fourier maps revealed the positions of all remaining non-hydrogen atoms. Phenyl rings were constrained to idealized hexagons, and the positions of the hydrogen atoms were calculated. The C–C and C–H distances were fixed at 1.395 and 0.95 Å, respectively, and the hydrogen atoms were constrained to "ride" on the carbon atoms to which they are attached. Isotropic thermal parameters were used for all but the non-hydrogen atoms of the $[Fe_{11}O_6(OH)_6]^{15+}$ core, carboxylate carbon atoms, and the non-hydrogen atoms of the well-behaved acetonitrile molecules (numbers 6 and 7), which were refined anisotropically. The positions of the hydrogen atoms of acetonitrile molecules numbered 1, 2, 5, and 6 were calculated, assuming tetrahedral geometry around the carbon atoms to which they are attached. The hydroxo hydrogen atoms were neither located nor calculated. Nine acetonitrile molecules were identified, but refinement of the site occupancy factors (SOF) for two of them (numbers 4 and 9) gave values close to 0.5. Their SOF were therefore fixed at 0.5, a linear geometry (observed in the difference Fourier maps) was imposed, and the thermal parameters were allowed to refine. High thermal parameters were obtained for methyl carbon atoms of MeCN numbers 1 and 2, indicating disorder and/or partial occupancy. Neutral atom scattering factors and anomalous dispersion corrections for non-hydrogen atoms were taken from ref 27 and hydrogen atom scattering factors from ref 28. The function minimized during the least-squares refinement was $\sum w(|F_o| - |F_c|)^2$. Blocked least-squares refinement[26] with unit weights converged to the discrepancy indices shown in Table I.

The eight acetonitrile molecules and one water molecule unambiguously located have been included in the molecular formula shown above. The fact that the elemental analysis only showed two acetonitrile molecules of crystallization is not surprising, since the crystals lose solvent rapidly unless sealed in capillaries with mother liquor. A final difference Fourier map revealed some residual electron density in the lattice, the largest peak having a height of 1.14 e Å^{-3}. Attempts to model this electron density as disordered solvent molecules were unsuccessful, perhaps accounting for the somewhat high final *R* values. The maximum value of the ratio of parameter shift to estimated standard deviation in the final refinement cycle was 1.6, for an acetonitrile solvent parameter, and at least two orders of magnitude smaller for all parameters of the $[Fe_{11}O_6(OH)_6(O_2CPh)_{15}]$ molecule. Oscillations of the solvent parameters about their equilibrium positions prevented full convergence, and refinement was stopped at this stage. Atomic positional parameters are presented in Table II, a list of bond distances and angles is given in Tables III and S7, and Tables S1–S3 list observed and calculated structure factors, thermal parameters for non-hydrogen atoms, and hydrogen atom positional and thermal parameters, respectively.

$[Fe_{11}O_6(OH)_6(O_2CPh)_{15}]$·6THF. The structure was solved by direct methods[23] in space group *C*2 with use of the Fe_{11} core atoms from the above structure determination as the trial solution. This approach was tried since the infrared and UV–visible spectral properties of the two crystalline forms proved to be similar. Space groups *Cm* and *C*2/*m* were eliminated since the point group of the molecule is D_3 and it sits on a special position. After the location of all non-hydrogen atoms from difference Fourier maps, their coordinates were transformed to space group *R*32 and refined with use of anisotropic thermal parameters for all but the phenyl ring carbon atoms. Hydrogen atoms and the phenyl rings were treated as described above for the triclinic form. Least-squares refinement converged to the *R* values shown in Table I. The weighting function used in the refinement was $w = 1.0/[\sigma^2(F_o) + 0.000625(F_o)^2]$. The largest residual peak in the final difference Fourier map was 1.74 e Å^{-3}, and it was not connected to the Fe_{11} molecule or to the hydrogen-bonded solvent. A peak of equal intensity was located on the 3-fold axis. Twelve peaks with interpeak distances less than 3.5 Å are located in a space large enough to contain a cylinder of diameter 15.5 Å and height 3 Å. These peaks, which have about half the electron density of a carbon atom on our maps, were tentatively assigned as crystallographically disordered or partially occupied solvent molecules. Attempts to refine them as MeCN, H_2O, or THF groups did not give sensible results, however, even when rigid molecular geometries or fractional site occupancy factors were employed. Although an accurate value of the density could not be determined because the crystals lose solvent rapidly,

(27) *International Tables for X-ray Crystallography*; Kynoch Press: Birmingham, England, 1974; Vol. IV, pp 99 and 149.
(28) Stewart, R. F.; Davidson, E. R.; Simpson, W. T. *J. Chem. Phys.* **1965**, *42*, 3175–3187.

Table II. Final Positional Parameters for $[Fe_{11}O_6(OH)_6(O_2CPh)_{15}]\cdot H_2O\cdot 8MeCN$ ($1\cdot H_2O\cdot 8MeCN$)[a]

ATOM	X	Y	Z	ATOM	X	Y	Z
Fe1	0.34960(10)	0.19130(10)	0.75620(10)	C65	0.0401(6)	0.3643(7)	0.3967(9)
Fe2	0.21060(10)	0.38000(10)	0.74790(10)	C66	0.1101(6)	0.3595(7)	0.4215(9)
Fe3	0.41270(10)	0.25760(10)	0.60380(10)	C77	0.4183(8)	0.4572(8)	0.7918(10)
Fe4	0.25690(10)	0.26800(10)	0.59930(10)	C71	0.4474(6)	0.5140(4)	0.8268(6)
Fe5	0.19740(10)	0.25220(10)	0.84830(10)	C72	0.4688(6)	0.5515(4)	0.7733(6)
Fe6	0.38460(10)	0.33420(10)	0.81040(10)	C73	0.4960(6)	0.6029(4)	0.8037(6)
Fe7	0.23730(10)	0.35980(10)	0.94980(10)	C74	0.5018(6)	0.6167(4)	0.8876(6)
Fe8	0.18520(10)	0.16020(10)	0.70840(10)	C75	0.4804(6)	0.5792(4)	0.9411(6)
Fe9	0.10930(10)	0.28260(10)	0.64990(10)	C76	0.4532(6)	0.5278(4)	0.9107(6)
Fe10	0.36680(10)	0.25840(10)	0.94910(10)	C87	0.2252(9)	0.4575(8)	0.6030(11)
Fe11	0.35830(10)	0.39270(10)	0.65300(10)	C81	0.1837(6)	0.4970(5)	0.5416(7)
O1	0.2524(5)	0.2013(5)	0.7704(7)	C82	0.1115(6)	0.5067(5)	0.5430(7)
O2	0.1108(6)	0.2841(5)	0.9132(7)	C83	0.0726(6)	0.5425(5)	0.4870(7)
O3	0.1947(6)	0.3155(5)	0.6721(7)	C84	0.1059(6)	0.5686(5)	0.4295(7)
O4	0.3661(5)	0.2569(5)	0.8324(6)	C85	0.1781(6)	0.5589(5)	0.4281(7)
O5	0.2335(6)	0.4471(5)	0.9484(6)	C86	0.2170(6)	0.5231(5)	0.4841(7)
O6	0.3271(6)	0.3251(5)	0.5735(6)	C97	0.2350(9)	0.4759(8)	0.8856(10)
O7	0.2140(5)	0.3330(5)	0.8413(6)	C91	0.2577(7)	0.5367(5)	0.8998(7)
O8	0.2847(6)	0.2098(6)	0.5016(7)	C92	0.2660(7)	0.5688(5)	0.8332(7)
O9	0.3104(6)	0.3696(5)	0.7393(6)	C93	0.2874(7)	0.6250(5)	0.8457(7)
O10	0.4320(6)	0.3214(5)	0.6985(6)	C94	0.3005(7)	0.6491(5)	0.9247(7)
O11	0.1864(6)	0.2102(6)	0.6091(6)	C95	0.2922(7)	0.6169(5)	0.9912(7)
O12	0.2209(6)	0.4593(6)	0.8125(7)	C96	0.2709(7)	0.5607(5)	0.9788(7)
O13	0.1875(6)	0.1748(5)	0.9038(7)	C107	0.5047(9)	0.1773(8)	0.7057(10)
O14	0.2744(6)	0.3648(5)	1.0681(7)	C101	0.5779(4)	0.1509(5)	0.7244(7)
O15	0.3625(6)	0.1295(6)	0.8415(7)	C102	0.5934(4)	0.1125(5)	0.7870(7)
O16	0.2621(6)	0.2642(5)	0.9521(6)	C103	0.6617(4)	0.0868(5)	0.8033(7)
O17	0.3440(6)	0.3517(5)	0.9253(6)	C104	0.7146(4)	0.0995(5)	0.7570(7)
O18	0.2421(6)	0.0953(6)	0.6477(7)	C105	0.6990(4)	0.1379(5)	0.6943(7)
O19	0.4156(6)	0.4184(5)	0.8410(7)	C106	0.6307(4)	0.1636(5)	0.6780(7)
O20	0.4593(6)	0.1684(5)	0.7531(7)	C117	0.0493(9)	0.3845(8)	0.7511(10)
O21	0.1915(6)	0.4356(6)	0.6515(7)	C111	-0.0111(6)	0.4158(5)	0.7999(7)
O22	0.1227(6)	0.2383(5)	0.7560(7)	C112	-0.0763(6)	0.3988(5)	0.7806(7)
O23	0.4928(6)	0.2036(6)	0.6396(7)	C113	-0.1332(6)	0.4255(5)	0.8242(7)
O24	0.0958(7)	0.1361(6)	0.6532(7)	C114	-0.1249(6)	0.4692(5)	0.8871(7)
O25	0.4743(6)	0.3001(5)	0.5393(7)	C115	-0.0596(6)	0.4862(5)	0.9064(7)
O26	0.1443(6)	0.3619(6)	0.9926(7)	C116	-0.0028(6)	0.4595(5)	0.8628(7)
O27	0.4868(7)	0.3089(5)	0.8559(7)	C127	0.1816(8)	0.1237(8)	0.8718(10)
O28	0.0402(6)	0.3421(6)	0.7000(7)	C121	0.1850(7)	0.0729(5)	0.9265(7)
O29	0.4673(6)	0.2603(5)	0.9648(7)	C122	0.2068(7)	0.0814(5)	1.0082(7)
O30	0.0393(6)	0.2266(6)	0.6481(7)	C123	0.2112(7)	0.0347(5)	1.0591(7)
O31	0.4317(6)	0.3979(5)	0.5689(7)	C124	0.1938(7)	-0.0206(5)	1.0284(7)
O32	0.2910(6)	0.4501(6)	0.5967(7)	C125	0.1720(7)	-0.0291(5)	0.9467(7)
O33	0.3991(6)	0.2103(5)	0.4966(7)	C126	0.1676(7)	0.0177(5)	0.8957(7)
O34	0.4010(6)	0.4562(6)	0.7171(7)	C137	0.3049(9)	0.0927(8)	0.6307(10)
O35	0.3796(6)	0.1746(5)	0.9683(6)	C131	0.3282(6)	0.0562(5)	0.5537(6)
O36	0.3621(6)	0.2868(5)	1.0713(7)	C132	0.3953(6)	0.0536(5)	0.5278(6)
O37	0.3403(6)	0.2354(5)	0.6592(6)	C133	0.4133(6)	0.0238(5)	0.4531(6)
O38	0.3518(6)	0.1158(5)	0.6740(7)	C134	0.3642(6)	-0.0034(5)	0.4044(6)
O39	0.2021(6)	0.3125(6)	0.5044(8)	C135	0.2970(6)	-0.0008(5)	0.4303(6)
O40	0.1060(7)	0.4068(6)	0.7675(7)	C136	0.2790(6)	0.0290(5)	0.5050(6)
O41	0.1714(6)	0.1088(6)	0.7960(7)	C147	0.4721(9)	0.3559(7)	0.5384(9)
O42	0.0910(6)	0.3120(6)	0.5409(8)	C141	0.5304(5)	0.3737(5)	0.4898(7)
C17	0.0467(10)	0.1712(9)	0.6240(11)	C142	0.5471(5)	0.4314(5)	0.5043(7)
C11	-0.0174(7)	0.1411(7)	0.5930(9)	C143	0.5995(5)	0.4492(5)	0.4618(7)
C12	-0.0158(7)	0.0795(7)	0.5926(9)	C144	0.6351(5)	0.4092(5)	0.4049(7)
C13	-0.0742(7)	0.0534(7)	0.5649(9)	C145	0.6183(5)	0.3514(5)	0.3904(7)
C14	-0.1342(7)	0.0891(7)	0.5376(9)	C146	0.5660(5)	0.3337(5)	0.4329(7)
C15	-0.1358(7)	0.1507(7)	0.5380(9)	C157	0.5065(9)	0.2756(7)	0.9119(10)
C16	-0.0774(7)	0.1768(7)	0.5657(9)	C151	0.5820(5)	0.2524(5)	0.9225(7)
C27	0.3217(8)	0.3312(8)	1.1005(10)	C152	0.6055(5)	0.2146(5)	0.9842(7)
C21	0.3331(6)	0.3460(5)	1.1931(5)	C153	0.6756(5)	0.1916(5)	0.9926(7)
C22	0.3695(6)	0.3048(5)	1.2441(5)	C154	0.7223(5)	0.2064(5)	0.9394(7)
C23	0.3802(6)	0.3209(5)	1.3269(5)	C155	0.6989(5)	0.2441(5)	0.8777(7)
C24	0.3545(6)	0.3781(5)	1.3586(5)	C156	0.6287(5)	0.2672(5)	0.8693(7)
C25	0.3181(6)	0.4193(5)	1.3076(5)	N1S1	0.2117(12)	0.2356(10)	0.1005(15)
C26	0.3074(6)	0.4032(5)	1.2248(5)	C2S1	0.1882(15)	0.2474(13)	0.1591(20)
C37	0.3418(9)	0.1973(8)	0.4676(9)	C3S1	0.1594(29)	0.2607(25)	1.2377(30)
C31	0.3401(6)	0.1638(6)	0.3850(6)	N1S2	0.1278(14)	0.1530(12)	0.4615(16)
C32	0.2790(6)	0.1435(6)	0.3539(6)	C2S2	0.0805	0.1507	0.4189
C33	0.2762(6)	0.1148(6)	0.2760(6)	C3S2	0.0327	0.1350	0.3656
C34	0.3344(6)	0.1064(6)	0.2291(6)	N1S3	0.4357(13)	0.6318(12)	0.2912(16)
C35	0.3955(6)	0.1268(6)	0.2601(6)	C2S3	0.4098(18)	0.5927(16)	0.249(2)
C36	0.3984(6)	0.1554(6)	0.3381(6)	C3S3	0.368(2)	0.551(2)	0.196(3)
C47	0.1020(8)	0.3267(8)	0.9656(10)	N1S4	-0.0822(18)	0.1437(19)	-0.022(3)
C41	0.0309(5)	0.3379(6)	1.0027(7)	C2S4	-0.0300(18)	0.1530(17)	-0.001(3)
C42	0.0224(5)	0.3690(6)	1.0787(7)	C3S4	0.0407(17)	0.1747(17)	0.024(2)
C43	-0.0424(5)	0.3779(6)	1.1128(7)	N1S5	0.237(3)	0.677(3)	0.282(4)
C44	-0.0985(5)	0.3558(6)	1.0709(7)	C2S5	0.256(3)	0.693(3)	0.347(4)
C45	-0.0900(5)	0.3247(6)	0.9949(7)	C3S5	0.305(3)	0.693(2)	0.412(3)
C46	-0.0253(5)	0.3158(6)	0.9608(7)	N1S6	0.3104(17)	0.825(2)	0.535(2)
C57	0.3749(8)	0.1293(8)	0.9781(10)	C2S6	0.3619(18)	0.8395(18)	0.5356(17)
C51	0.3851(6)	0.0683(4)	0.9525(6)	C3S6	0.4289(16)	0.8623(18)	0.5365(19)
C52	0.4139(6)	0.0615(4)	1.0313(6)	N1S7	0.9969(12)	0.2043(12)	0.7979(13)
C53	0.4250(6)	0.0052(4)	1.0620(6)	C2S7	-0.0563(16)	0.1939(15)	0.7930(16)
C54	0.4074(6)	-0.0443(4)	1.0139(6)	C3S7	-0.1315(16)	0.178(3)	0.778(2)
C55	0.3786(6)	-0.0375(4)	0.9351(6)	N1S8	0.4733(17)	0.0195(15)	0.730(2)
C56	0.3674(6)	0.0188(4)	0.9044(6)	C2S8	0.440(3)	-0.032(3)	0.724(3)
C67	0.1378(10)	0.3254(8)	0.4959(11)	C3S8	0.389(4)	-0.071(3)	0.715(4)
C61	0.1547(6)	0.3891(7)	0.3818(9)	N1S9	0.122(4)	0.010(3)	0.247(4)
C62	0.1292(6)	0.4235(7)	0.3172(9)	C2S9	0.076(4)	0.006(3)	0.207(5)
C63	0.0591(6)	0.4283(7)	0.2923(9)	C3S9	0.015(4)	-0.009(4)	0.147(5)
C64	0.0146(6)	0.3987(7)	0.3321(9)	O1w	0.203(3)	0.947(3)	0.689(3)

[a] Atoms are labeled as shown in Figure 3. Estimated standard deviations, in parentheses, occur in the last significant digit(s) for each parameter.

it was estimated to be around ~1.3 g/cm³ from neutral buoyancy studies in aqueous KI. This value is higher than the calculated value of 1.1 g/cm³, supporting the notion that additional solvent occurs in the crystal lattice. Since only six THF molecules were unambiguously located, the formula of this crystalline form has been assigned as $[Fe_{11}O_6(OH)_6(O_2CPh)_{15}]\cdot 6THF$.

Twelve reflections for which $F_o \sim 0.5F_c$, possibly due to the effect of secondary extinction and/or missing electron density in the model, were

Table III. Selected Interatomic Distances (Å) and Angles (deg) for $[Fe_{11}O_6(OH)_6(O_2CPh)_{15}]$ (**1**) in **1**·H_2O·$8CH_3CN$ (A) and **1**·6THF (B)[a,b]

	iron coordination spheres					
	A			B[c]		
	min	max	mean	min	max	mean
Type A Iron						
Fe–O(μ-oxo)	1.90 (1)	1.94 (1)	1.92 (2)			1.925 (6)
Fe–O(benzoate)	2.04 (1)	2.13 (1)	2.08 (3)			2.106 (8)
O(μ-oxo)–Fe–O(μ-oxo)	93.8 (5)	96.7 (5)	95.0 (1.0)			95.9 (2)
O(μ-oxo)–Fe–O(benzoate)						
cis	84.7 (5)	87.7 (5)	87.1 (1.2)			87.0 (3)
	93.7 (5)	96.3 (5)	95.0 (9)			94.2 (3)
trans	168.0 (5)	171.3 (4)	169.7 (1.1)			169.2 (3)
O(benzoate)–Fe–O(benzoate)	81.9 (5)	83.9 (5)	82.6 (8)			82.4 (3)
Type B Iron						
Fe–O(μ-oxo)	1.88 (1)	1.93 (1)	1.907 (18)			1.876 (5)
Fe–O–(μ-hydroxo)	2.03 (1)	2.16 (1)	2.11 (4)			2.051 (8)
Fe–O(benzoate)	1.93 (1)	2.07 (1)[d]	1.99 (4)	1.967 (7)	2.036 (6)[d]	2.004 (28)
O(μ-oxo)–Fe–O(μ-hydroxo)	77.6 (4)[e]	94.1 (4)	85.0 (7.4)	77.5 (2)[e]	93.1 (3)	85.3 (7.8)
O(μ-oxo)–Fe–O(benzoate)						
trans	163.1 (5)	165.9 (5)	164.1 (9)			162.5 (3)
cis[f]	95.1 (5)	105.3 (5)	100.1 (4.1)	95.3 (3)	104.5 (3)	99.9 (4.6)
O(μ-hydroxo)–Fe–O(μ-hydroxo)	81.7 (4)	83.8 (5)	82.8 (7)			83.2 (3)
O(benzoate)–Fe–O(benzoate)	83.6 (5)	96.2 (5)	90.3 (3.5)	85.2 (3)	92.9 (3)	90.1 (3.5)
O(μ-hydroxo)–Fe–O(benzoate)						
trans	167.0 (5)	175.5 (5)	171.0 (2.1)	170.5 (2)	173.1 (4)	171.8 (1.3)
cis	83.1 (4)	96.6 (5)	88.6 (3.8)	85.0 (2)	94.2 (3)	88.7 (3.7)
Type C Iron						
Fe–O(μ-oxo)	1.91 (1)	1.93 (1)	1.920 (8)			1.926 (7)
Fe–O(μ-hydroxo)	2.06 (1)	2.10 (1)	2.083 (12)			2.078 (6)
Fe–O(benzoate)	2.05 (1)	2.10 (1)	2.080 (19)			2.083 (8)
O(μ-oxo)–Fe–O(μ-oxo)	108.5 (5)	109.5 (5)	108.9 (4)			107.8 (4)
O(μ-hydroxo)–Fe–O(μ-hydroxo)	172.0 (5)	175.0 (5)	173.3 (1.3)			175.5 (4)
O(benzoate)–Fe–O(benzoate)	79.2 (5)	81.3 (5)	80.0 (9)			80.4 (4)
O(μ-oxo)–Fe–O(benzoate)						
cis	86.7 (5)	90.4 (5)	88.5 (1.3)			88.7 (3)
trans	154.2 (5)	158.2 (5)	156.9 (1.4)			157.3 (3)
O(μ-hydroxo)–Fe–O(benzoate)[f]	79.4 (5)	95.4 (5)	87.5 (6.3)	82.9 (3)	93.7 (3)	88.3 (5.4)
O(μ-oxo)–Fe–O(μ-hydroxo)[f]	78.0 (5)	106.7 (4)	92.0 (13.1)	77.9 (2)	104.8 (2)	91.4 (13.5)
	angles about bridging oxygens					
	A			B[c]		
FeA–O(μ-oxo)–FeB	125.0 (6)	127.2 (6)	126.4 (7)			126.4 (4)
FeA–O(μ-oxo)–FeC	128.5 (6)	131.0 (6)	129.8 (8)			129.2 (3)
FeB–O(μ-oxo)–FeC	102.9 (6)	104.8 (5)	103.8 (8)			104.4 (3)
FeB–O(μ-hydroxo)–FeB	95.0 (5)	98.0 (5)	96.4 (10)			96.0 (3)
FeB–O(μ-hydroxo)–FeC[f]	89.6 (4)	126.5 (6)	107.6 (17.0)	90.0 (9)	125.4 (3)	107.7 (17.7)

[a] For **1**·H_2O·$8CH_3CN$ (A), atoms are labeled as shown in Figure 2. For both A and **1**·6THF (B), iron atom label types A, B, C are defined in Figure 1. [b] Estimated standard deviations in individual values are given in parentheses. For mean values, $\sigma = [\sum x^2 - n\bar{x}^2)/n]^{1/2}$. [c] When no "min" or "max" values are given, there is only one crystallographically independent bond distance or angle, which is reported under the column designated "mean". [d] The longer bonds are trans to the μ-oxo ligand. [e] The smaller angles are part of a 4-membered ring. [f] There are two classes of angles that involve different bond types that can be discerned from Figure 2 and/or Tables S7 and S8, which contain a full list of bond distances and angles for **1** and the solvent molecules.

omitted from the final refinement. The absolute configuration in space group *R*32 was determined by performing a Hamilton test[29] at the 0.005 confidence level. The maximum value of the ratio of parameter shift to estimated standard deviation was 0.003 for the thermal parameters of the carbon atoms in the THF molecule and ≤0.001 for the rest of the parameters. Final non-hydrogen atomic positional parameters are given in Table IV, molecular geometry in Tables III and S8, observed and calculated structure factor amplitudes in Table S4, thermal parameters for non-hydrogen atoms in Table S5, and hydrogen atom parameters in Table S6.

Magnetic Susceptibility Measurements. Solid-state magnetic measurements were carried out with methods described previously.[16b] A powdered sample of **1**·6THF was kept under vacuum for 24 h until constant weight was achieved. Elemental analysis showed no residual solvent. Variable field and temperature magnetic susceptibility measurements were carried out with a S.H.E. Model 905 SQUID-type susceptometer. Magnetization studies were conducted at 5 and 2.5 K in fields up to 50 kOe with 30 mg of sample and, in these cases, the diamagnetic correction, which accounts for less than 0.5% of the observed moments, was neglected. Magnetization experiments at 4.2 K and 1.3 K employing fields up to 230 kOe were performed by using a vibrating sample magnetometer (VSM).[30] The diamagnetic contributions of the sample and holder to the magnetic moment were negligibly small and were not included in the calculations. Variable temperature magnetic susceptibility data were collected at 5 kOe between 5.0 and 300 K and processed as described previously.[16a]

Infrared and Optical Spectroscopy. Infrared spectra in the range 400–4000 cm^{-1} were recorded with a Beckman Acculab 10 instrument and an IBM IR/32 FT instrument. Electronic spectra in the range 220–800 nm were recorded with a Perkin-Elmer Model 230B spectrophotometer and with a Perkin-Elmer Model 300 up to 1500 nm.

Mössbauer Spectroscopy. Mössbauer spectra of polycrystalline samples of **1** were recorded at temperatures varying from 2 to 290 K and in longitudinal magnetic fields of up to 80 kOe at 4.2 K. Isomer shifts were measured relative to iron metal at 300 K. Two different samples, including one that was analyzed, gave identical results.

(29) Hamilton, W. R. *Acta Crystallogr.* **1965**, *18*, 502–510.

(30) Foner, S.; McNiff, E. J., Jr. *The Review of Scientific Instruments* **1968**, *39*, 171–179.

Table IV. Final Positional Parameters for $[Fe_{11}O_6(OH)_6(O_2CPh)_{15}]\cdot 6THF$ (1·6THF)[a]

ATOM	X	Y	Z
Fe1	0.0000	0.0000	-0.04997(4)
Fe2	-0.13943(9)	0.0000	0.0000
Fe3	-0.19069(8)	-0.15976(8)	-0.03163(3)
O1	-0.1028(4)	-0.0494(4)	-0.02872(11)
O2	-0.1257(4)	-0.2067(4)	-0.01066(11)
O3	-0.2712(4)	-0.1303(5)	-0.04961(13)
O4	-0.2293(4)	-0.0080(4)	-0.02868(14)
O5	-0.1713(4)	-0.1996(4)	-0.06835(13)
O6	-0.0421(5)	-0.0994(5)	-0.07929(12)
O7	-0.2937(4)	-0.2715(4)	-0.02270(15)
C17	0.0646(8)	-0.2079(7)	-0.0466(2)
C11	0.0484(5)	-0.2788(5)	-0.06555(15)
C12	-0.0302(5)	-0.3502(5)	-0.06640(15)
C13	-0.0448(5)	-0.4161(5)	-0.08448(15)
C14	0.0194(5)	-0.4106(5)	-0.10171(15)
C15	0.0980(5)	-0.3392(5)	-0.10086(15)
C16	0.1125(5)	-0.2733(5)	-0.08278(15)
C27	-0.1070(8)	-0.1711(7)	-0.0831(2)
C21	-0.1010(6)	-0.2201(5)	-0.10682(14)
C22	-0.0256(6)	-0.1955(5)	-0.12082(14)
C23	-0.0217(6)	-0.2446(5)	-0.14277(14)
C24	-0.0932(6)	-0.3183(5)	-0.15072(14)
C25	-0.1685(6)	-0.3429(5)	-0.13672(14)
C26	-0.1725(6)	-0.2938(5)	-0.11477(14)
C37	0.3130(8)	0.0000	0.0000
C31	0.3948(8)	0.0000	0.0000
C32	0.4511(6)	0.0364(8)	0.0227(3)
C33	0.5250(7)	0.0336(10)	0.0218(3)
C34	0.5428(10)	0.0000	0.0000
O1S	-0.1992(6)	-0.3776(5)	-0.0231(2)
C1S	-0.1999(11)	-0.4312(10)	-0.0020(3)
C2S	-0.2450(16)	-0.5159(12)	-0.0163(6)
C3S	-0.2875(17)	-0.5130(12)	-0.0406(6)
C4S	-0.2538(11)	-0.4286(10)	-0.0475(3)

[a] Atoms are labeled as described in Table III. Numbers in parentheses are estimated standard deviations in the last significant digit(s).

Electrochemistry. Cyclic voltammetry experiments were carried out with a Princeton Applied Research (PAR) Model 173 Potentiostat, a PAR Model 175 Universal Programmer, a PAR Model 179 Digital Coulometer and a Houston Instrument Model 2000 X-Y Recorder. Measurements were made on 4×10^{-4} M solutions of $[Fe_{11}O_6(OH)_6(O_2CPh)_{15}]$ dissolved in methylene chloride with 0.2 M tetra-*n*-butylammonium perchlorate, triply recrystallized from ethyl acetate/pentane as the supporting electrolyte. All experiments were performed at 24–25 °C under a nitrogen atmosphere. A three-electrode system consisting of a platinum disc working electrode, a platinum wire auxiliary electrode, and a Ag/AgCl reference electrode was employed for all measurements, and the values were converted to the more conventional saturated calomel electrode by adding 0.019 V. The measurement of the Fe(0/+) couple of ferrocene was used to check the performance of the system and yielded a half-wave potential of +0.48 V and a peak-to-peak separation of 110 mV at a scan rate of 200 mV/s.

Results and Discussion

Synthesis. Both the aquo-acetonitrile and the THF solvates of $[Fe_{11}O_6(OH)_6(O_2CPh)_{15}]$ (**1**) were obtained by diffusing water into anhydrous acetonitrile solutions of iron(III) in the presence of carboxylate anions. The introduction of water by liquid–liquid diffusion with aqueous THF gave better and more reproducible results than did vapor diffusion. The crystals obtained were of X-ray quality and were stored under solvent. Despite the fact that THF is hydrogen bonded to the Fe_{11} aggregate (see below), drying the powdered crystals in vacuo at room temperature overnight removed all solvent as demonstrated by elemental analysis. The complex is stable indefinitely as a dried solid and as a solution in MeCN or CH_2Cl_2 for at least 1 week, as determined by optical spectroscopy.

The factors that determine the extent of hydrolytic polymerization of Fe(III) have not been fully delineated. In the present study, an oxo/hydroxo-bridged undecairon aggregate was obtained when limited quantities of water were used to hydrolyze and polymerize an unknown intermediate (X) which forms when stoichiometric amounts of $[Fe_2OCl_6]^{2-}$ and sodium benzoate are mixed. Compound **1** is obtained in nonaqueous solvents only with slow addition to intermediate X, or to X plus an equivalent of $[FeCl_4]^-$, of H_2O as hydrolyzing and polymerizing agent. These procedures are similar to those employed in the stepwise formation of the $\{Fe_3O\}^{7+}$ core described previously.[16] An increase in the amount of water present or quicker diffusion leads mostly to flocculent brown precipitates. Even under optimal conditions, a small amount of amorphous precipitate is formed, but this material can be easily separated from the crystals, as described in the Experimental Section. The clear solution that remains after the removal of the solids still contains iron.

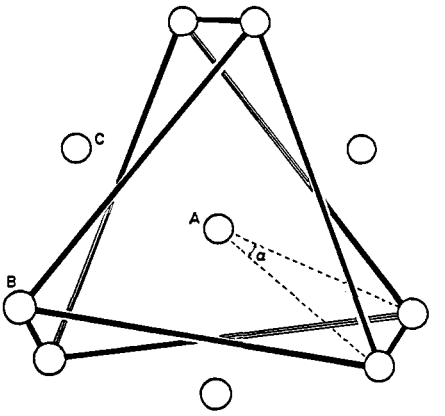

Figure 1. Arrangement of iron atoms in **1** viewed down the C_3 symmetry axis. The top and bottom iron atoms are eclipsed. Labels A, B, and C refer to the three distinct iron atom types in the aggregate (see text). The twist angle α is defined in the text.

Addition of potassium hydrotris(1-pyrazolyl)borate ($KHBpz_3$) to intermediate X described above leads to the hemerythrin model complex, (μ-oxo)bis(μ-benzoato)bis[hydrotris(1-pyrazolyl)borato]diiron(III), $[Fe_2O(O_2CPh)_2(HBpz_3)_2]$ (**2**).[31] This complex is precipitated from the reaction mixture with excess H_2O, and it does not hydrolyze appreciably within 1 h upon stirring the aqueous heterogeneous mixture. Attempts to prepare **2** in aqueous solution, using sodium benzoate and ferric perchlorate, gave only the bis(chelate) iron(III) complex, $[Fe(HBpz_3)_2]^+$, with no benzoate incorporated.[31,32] Once **2** is assembled from the preformed (μ-oxo)diiron(III) unit, however, its integrity is preserved in aqueous mixtures. Moreover, the formate and acetate analogues of **2** decompose slowly in water to form $[Fe(HBpz_3)_2]^+$.[18] All of these results suggest a hydrophobic role for the phenyl residues in limiting the hydrolysis of iron(III) complexes in aqueous solutions.

Finally, it may be noted that hydrolysis of inorganic iron salts in water, in the presence of carboxylate anions, gives a mixture of structurally uncharacterized polymers, sometimes referred to as the "Spiro-Saltman ball", with properties resembling those of the ferritin core.[10] A comparison between the mode of formation of $[Fe_{11}O_6(OH)_6(O_2CPh)_{15}]$ and the ferritin core is made below.

Description of the Structure. The structure of $[Fe_{11}O_6(OH)_6(O_2CPh)_{15}]$ is nearly the same in both crystallographic forms. The eleven iron atoms are situated at the vertices of a twisted, pentacapped trigonal prism which is slightly distorted in the triclinic space group but has crystallographically required D_3 symmetry in the trigonal form. A view of this arrangement of iron atoms down the C_3 axis is depicted in Figure 1. There are three chemically distinct types of iron atoms in the aggregate. Type A iron atoms cap the triangular faces of the twisted trigonal prism and are situated on the C_3 axis in the trigonal form. There are two type A iron atoms, each bonded to three benzoate oxygen atoms and the triply bridging μ_3-oxo oxygen atoms. In the triclinic form, the type A iron atoms are labeled Fe1 and Fe2, as shown in Figure 2 which displays the full structure except for the benzoate group carbon atoms. Six type B iron atoms define the body of the twisted trigonal prism (Figure 1) and are all symmetry related to one another in the trigonal form. These six atoms, labeled Fe3, Fe7, Fe8, Fe9, Fe10, and Fe11 in the triclinic form (Figure 2), are each coordinated to three benzoate oxygen atoms occupying an octahedral face, two cis μ_3-hydroxo oxygen atoms, and one μ_3-oxo oxygen atom. The remaining three, type C, iron atoms are situated on C_2 axes in the trigonal form and are labeled as

(31) Armstrong, W. H.; Spool, A.; Papaefthymiou, G. C.; Frankel, R. B.; Lippard, S. J. *J. Am. Chem. Soc.* **1984**, *106*, 3653–3667 and references cited therein.

(32) For analogous TACN complexes, see: Wieghardt, K.; Pohl, K.; Gebert, W. *Angew. Chem., Int. Ed. Engl.* **1983**, *22*, 727.

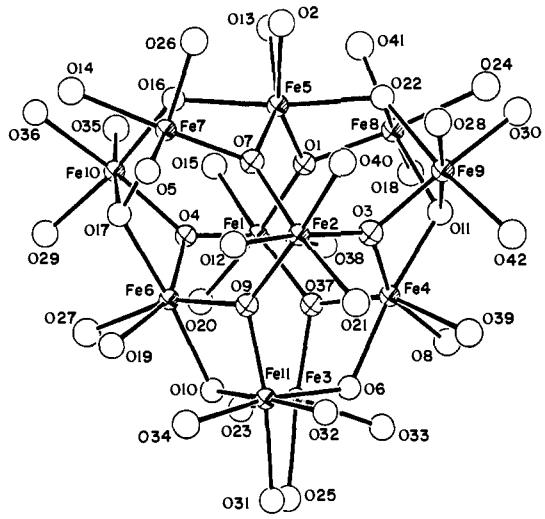

Figure 2. Structure of **1** in the triclinic form, showing the 40% probability thermal ellipsoids and atom labels for iron and oxygen atoms. All carbon atoms of the benzoate groups are omitted.

Fe4, Fe5, and Fe6 in the triclinic crystal (Figures 1 and 2). They are each bonded to two cis μ_3-oxo, two trans μ_3-hydroxo, and two cis benzoate oxygen atoms.

As shown in Figure 1, twist angle α is defined as the angle between vectors connecting type A and B iron atoms on the upper and lower corners of the twisted trigonal prism projected onto the mean plane through the prism. In the triclinic form, the values for α are 16.2, 16.9, and 19.9° (average 17.7°), comparable to the value of 17.4° for α in the trigonal structure. The nonzero value of the twist angle α is the natural consequence of the topological linking of type A, B, and C iron atoms by means of μ_3-oxo and μ_3-hydroxo bridge bonds, described in more detail below.

Table III summarizes details of the iron coordination geometries in $[Fe_{11}O_6(OH)_6(O_2CPh)_{15}]$. The shortest Fe–O bonds are those involving μ_3-oxo ligands, with the 1.876 (6) Å value for the type B iron atoms being significantly (Δ/σ = 6) shorter than the respective values of 1.925 (6) and 1.926 (7) Å for type A and C iron atoms.[33] This difference may be due to the fact that type B iron atoms are coordinated to only one oxo ligand, whereas the other types have two or three such donor atoms. The Fe–O bonds involving the benzoate groups range from 1.967 (7) to 2.083 (8) Å, the longer distances consistently being those trans to the μ_3-oxo ligand. The average value of 2.06 (5) Å is the same as that found for the Fe–OH bonds, 2.064 (14) Å.

In both crystallographic forms of **1**, the iron atoms situated on the twofold symmetry axes (type C) have intrabond angles quite distorted from regular octahedral values (Figure 2). This distortion may be defined by the dihedral angle between planes (μ_3-oxo)–Fe–(μ_3-oxo) and (benzoate O)–Fe–(O benzoate), for example, O1–Fe5–O7 and O2–Fe5–O13. The dihedral angles deviate from the idealized value of zero degrees by 25.1° in the trigonal form and by 26.8, 24.8, and 25.4° (25.7° average) in the triclinic form.

The distances from the center of the aggregate to the iron atoms are 2.331 (2) Å for two type A irons on the C_3 axis, 3.599 (1) Å for six type B iron atoms, and 2.582 (2) Å for three type C irons on C_2 axes. Thus, the pentacapped trigonal prism formed by the 11 iron atoms can be inscribed by a sphere of radius 3.6 Å. Further stereochemical information is given in Table III; alternative descriptions of the undecairon aggregate may be found in ref 19 and 34.

The 12 μ_3-oxo and μ_3-hydroxo oxygen atoms form an irregular icosahedron with a close-packed, antiprismatic arrangement of the six μ_3-oxo atoms at the core (Figure 3). Although the hydrogen atoms of the hydroxyl groups were not crystallographically located, an unambiguous assignment of the μ_3-oxo vs. μ_3-hydroxo oxygens was made on the basis of several criteria. The average Fe–(μ_3-oxo) distances are, as shown above, the shortest of the three kinds, as expected for such bonds. Moreover, the sum of Fe–O–Fe angles is 360° around the planar μ_3-oxo and 312° around the nonplanar μ_3-hydroxo groups. These sums are expected to be 360° and 328.4°, respectively, for pure sp^2 and sp^3 hybridized atoms. In the trigonal form, six ordered THF molecules are hydrogen bonded to the hydroxo ligands (vide infra) with an O(H)···O(THF) distance of 2.78 Å. Four acetonitrile molecules in the triclinic form are also hydrogen bonded to the hydroxo groups at O(H)···N distances ranging from 2.82 to 2.91 Å. Finally, an O–H stretching mode is observed ~3600 cm^{-1} in the infrared spectrum of desolvated **1**, confirming the presence of hydroxo ligands in the aggregate.

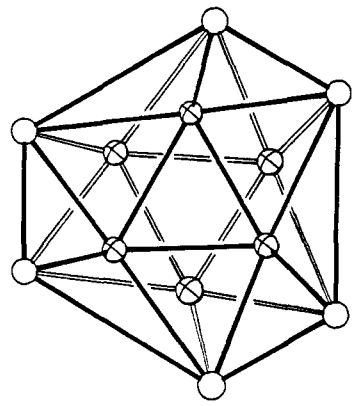

Figure 3. The distorted icosahedron of oxygen atoms in **1** viewed down the C_3 symmetry axis. Spherical crosses and open circles denote the μ_3-oxo and μ_3-hydroxo oxygen atoms, respectively.

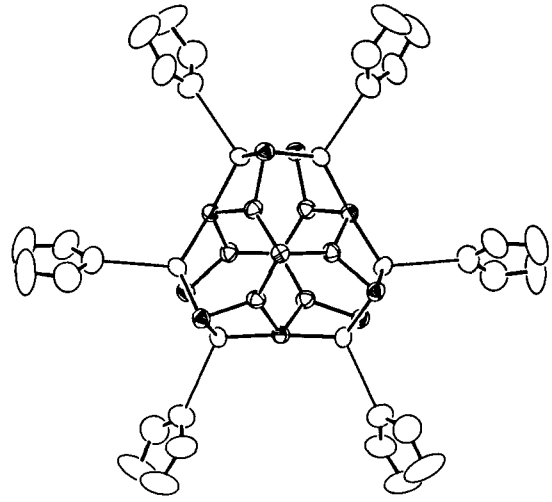

Figure 4. Structure of the $\{Fe_{11}O_6(OH)_6\}^{15+}$ core in **1**·6THF, illustrating the hydrogen bonding of six solvent molecules to the μ_3-hydroxo groups.

Nine FeO_6 octahedra, comprised of six type B and three type C iron centers, are joined by corner sharing oxygen atoms into a large nonplanar ring that is capped above and below by the two additional type A FeO_6 octahedra situated on the C_3 axis. This kind of condensation has been proposed for the polymerization of $[Fe(H_2O)_6]^{3+}$ ions when μ_3-oxo and μ_3-hydroxo bridges are formed in vitro and possibly in vivo.[9] The 15 bridging benzoate groups provide a hydrophobic sheath around the aggregate, limiting further growth or linking of aggregates by bridging ligands. In contrast to $\{Fe_2O\}^{4+}$, symmetrical $\{Fe_3O\}^{7+}$, and $\{Fe_4O_2\}^{8+}$ cores, no two benzoate groups bridge the same pair of iron atoms.[12,17,31,34] A similar situation obtains in the asymmetric $\{Fe_3O\}^{7+}$ core in $[Fe_3O(TIEO)_2(O_2CPh)_2Cl_3]$.[16] Protruding through the hydro-

(33) Geometric comparisons within the $[Fe_{11}O_6(OH)_6(O_2CPh)_{15}]$ aggregate will be made only for the more precisely determined trigonal crystallographic form. Results for the triclinic form are qualitatively similar (see Tables III, S7, and S8).

(34) Lippard, S. J. *Chem. Brit.* **1986**, 222–229.

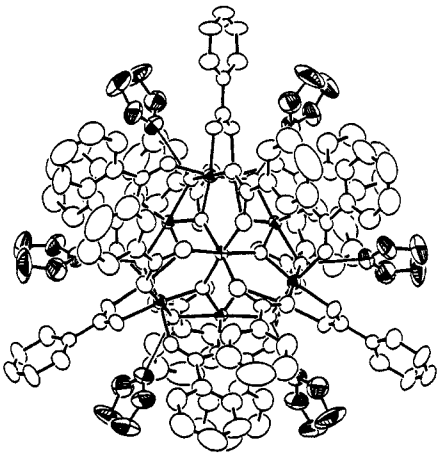

Figure 5. Full structure of **1**·6THF, showing the 40% probability thermal ellipsoids.

phobic sheath of benzoate groups, however, are the six protons of the μ_3-hydroxo ligands which, in the case of **1**·6THF, form hydrogen bonds to the tetrahydrofuran solvent molecules (Figures 4 and 5). Packing diagrams of the $[Fe_{11}O_6(OH)_6(O_2CPh)_{15}]$·6THF structure may be found in ref 17a.

Geometric Speculations about the Ferritin Core. It is interesting to speculate about the possibility that the ferritin core is filled with aggregates of average composition $\{Fe_{11}O_6(OH)_6\}X_{15}$, X = bridging and/or terminal OH^- and/or X = $0.5HPO_4^{2-}$, where the monohydrogen phosphate groups are bidentate and/or bridging. If we define the internal diameter of the ferritin shell to be $2R$, the volume is $V = 4\pi R^3/3$. The volume of the sphere encapsulating the Fe_{11} aggregate is $v = 4\pi r^3/3$, where r is its radius. This latter radius may be defined in two ways. The distance from the geometric center of the $[Fe_{11}O_6(OH)_6(O_2CPh)_{15}]$ aggregate to the midpoint between the OH oxygen and THF oxygen atoms is 5.27 Å, the "hydrogen bond" radius of the sphere encapsulating the Fe_{11} core. Similarly, a "covalent bond" radius of 4.5 Å may be defined as the distance from the center of the aggregate to the midpoint between the outermost iron and benzoate oxygen atoms. If fully loaded ferritin has m iron atoms composed of n clusters, each with p iron atoms, then eq 3 and 4 obtain. For R = 35–40

$$r = R(p/m)^{1/3} \quad (3)$$

$$n = (R/r)^3 \quad (4)$$

Å, p = 11, and m = 4500 (fully loaded ferritin),[4,6] r = 4.7–5.4 Å, which compares favorably with the covalent and hydrogen bond radii of **1**. A total of 409 ± 3 Fe_{11} units are necessary to fill the entire core.

It is important to realize that the calculation of the maximum number of iron atoms present in the core of horse spleen ferritin, and hence the value of r, is based on a measurement of its sedimentation coefficient[6g] and the formula $[(FeOOH)_8(FeO_2PO_2H_2)]$. If the phosphate anions are not included, then m increases in the above calculation and r diminishes toward the covalent bond value (eq 3). On the other hand, a more recent measurement of the number of iron atoms present in the ferritin core, based upon the X-ray absorption of single crystals of ferritin, yielded a value of 2100 ± 150.[6h] Since this number was for a "statistically half-full molecule", a full molecule would have 4200 ± 300 iron atoms, assuming the same relative error, which would tend to increase r toward the hydrogen bond radius. The replacement of phosphate anions by oxo or hydroxo ligands is conceptually legitimate, since ferritin cores reconstituted in the absence of phosphate exhibit the same diffraction pattern as cores from native ferritin.

Since 60–80% of the phosphate present in horse spleen ferritin is adventitious (i.e., surface bound[6f]), only 20–40% of the phosphate is presumably an integral part of the core and available to bridge polyiron aggregates. That is, there are 11–23 iron atoms per crystallite, assuming the phosphate only bridges two such units.

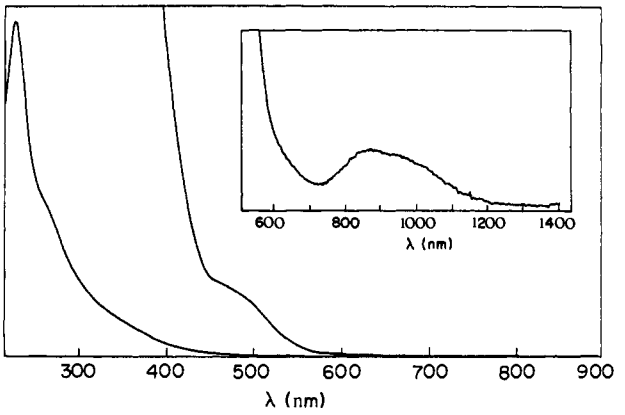

Figure 6. Optical spectrum of **1**·6THF in CH_2Cl_2.

Using the recently measured ratio Fe/P = 21.0 for human thalassemic ferritin cores,[6i] one may calculate 10–11 iron atoms per crystallite. Whether or not 11 iron atoms is a "magic number" for the building blocks of the ferritin core remains to be established.

Considering the approximations, the foregoing calculations cannot distinguish between two extreme models for the ferritin core, one of which involves only covalent bonds and a single isotropic crystallite, and the other of which involves hydrogen-bonded or, if their number is not too high, phosphate-linked microcrystallites in a sponge-like array. Since r is proportional to the cubic root of the p/m ratio, however, it is not very sensitive to the approximations made. The very fact that $[Fe_{11}O_6(OH)_6(O_2CPh)_{15}]$, with its $\{Fe_{11}O_6(OH)_6\}^{15+}$ core, spontaneously self-assembles is in itself some reason to speculate that Fe_{11} units may be involved as structural components of the ferritin core. After all, $Fe_nS_n^{x-}$ clusters were known in inorganic chemistry prior to their discovery in biology.[35]

Infrared and Electronic Spectra. Except for the assignment of the 3600-cm^{-1} peak as a ν_{OH} stretching mode (vide supra), the vibrations of the $\{Fe_{11}O_6(OH)_6\}^{15+}$ core cannot be identified with certainty without isotopic substitution studies. Strong infrared spectral bands at 1597, 1557, and 1413 cm^{-1} originate in the bridging benzoate groups and are also present in benzoate complexes containing the $\{Fe_2O\}^{4+}$, $\{Fe_3O\}^{7+}$, and $\{Fe_4O_2\}^{8+}$ cores.[16,31] The electronic spectrum of **1** in CH_2Cl_2 (Figure 6) is dominated by strong absorptions from the phenyl group and by ligand-to-metal charge-transfer bands. The positions and the approximate intensity of the shoulders below 490 nm suggest a charge transfer transition, similar to what has been proposed for Hr, Ft, and related iron oxo/hydroxo polymers.[10,11,36] A prominent shoulder at 492 nm with an "extinction coefficient" per iron of 137 M^{-1} cm^{-1} could be a charge transfer band, an enhanced $^6A_1 \rightarrow [^4A_1,^4E](^4G)$ ligand field transition, or both. This shoulder shifts to 480 nm in acetonitrile and, in both solvents, remains unchanged for at least 1 week. This result differs from the behavior of iron(III) salts upon hydrolysis in aqueous solution. A shoulder at 470 nm in the optical absorption spectrum increases in intensity as the initially formed polymers age. The formation of oxo bridges from condensation of hydroxyl groups is thought to be responsible for this change.[11] In the present case, the phenyl rings probably limit the extent of growth of the polymer and, consequently, the aging phenomenon. The intensity of the 490-nm band is two orders of magnitude higher than expected for a ligand field band, even one enhanced by low symmetry or magnetic interactions. The 490-nm band is a shoulder on an underlying transition, however, so its true intensity is difficult to estimate. The broad peak observed in the near-IR region of the spectrum at 881 nm, with an extinction coefficient of ~6 M^{-1} cm^{-1}, might be an enhanced d–d band, possibly $^6A_1 \rightarrow {}^4T_1(^4G)$. A similar band is observed in the synthetic iron polymer of approximate composition $[Fe_4O_3(OH)_4(NO_3)_2]$·$1.5H_2O$,[10b] and in ferritin[36] at 900 nm with

(35) Beinert, H. In *Iron–Sulfur Proteins*; Lovenberg, W., Ed.; Academic Press: New York, 1973; Vol. I, pp 1–36.
(36) Webb, J.; Gray, H. B. *Biochim. Biophys. Acta* **1974**, *351*, 224–229.

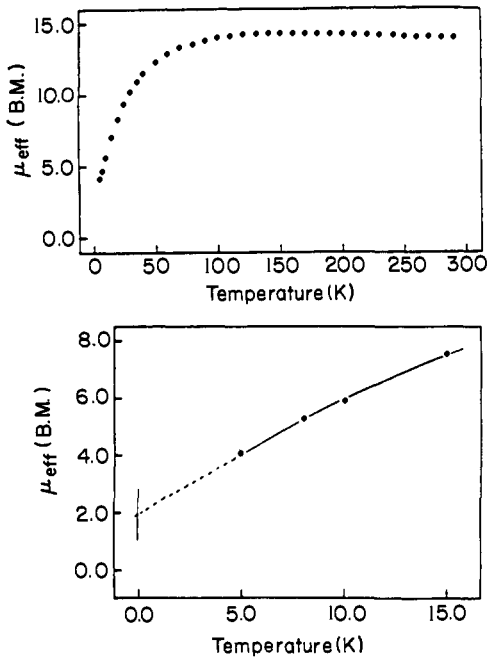

Figure 7. Temperature dependence of the effective magnetic moment per aggregate of **1**. The top panel shows the full temperature range. The bottom panel is an expanded version of the low-temperature data, including an extrapolation to 0 K.

extinction coefficients of 4.4 M^{-1} cm^{-1}. This absorption band has been used to establish the predominance of octahedrally coordinated Fe^{3+} in ferritin.

Magnetic and Mössbauer Studies. The results of variable temperature magnetic susceptibility studies of **1** are presented in Figure 7. The values of μ_{eff} were calculated from the spin-only formula, eq 5, where χ_M is the molar susceptibility. The reduction

$$\mu_{eff} = 2.828(\chi_M T)^{1/2} \quad (5)$$

in the effective magnetic moment from 13.92 μ_B per Fe_{11} molecule, or 4.2 μ_B per iron, at 298 K, to 3.32 μ_B per molecule (1.0 μ_B per iron) at 2.6 K is indicative of net antiferromagnetic coupling within the aggregate. Extrapolation of the μ_{eff} vs. T curve to 0 K yields a value of ~1.9 μ_B per aggregate, approaching the theoretical value of 1.73 μ_B for a ground state with $S_T = {}^1/_2$. In principle, 11 ferric ions with spin ${}^5/_2$ can couple to give total spins ranging from ${}^1/_2$ to ${}^{55}/_2$. The rapid rise in effective moment with temperature, ~0.36 μ_B K^{-1}, at low temperature implies the existence of low-lying magnetic excited states. This situation is not unexpected, since there are 27 nearest neighbor pairwise interactions among the 11 iron(III) centers in the aggregate. Because of the bulky benzoate ligands, there are no significant interactions between $[Fe_{11}O_6(OH)_6(O_2CPh)_{15}]$ molecules in the lattice. The magnetic domain is thus limited to the undecairon aggregate itself.

Further insight is provided by the results of high field magnetization studies of **1** at 1.3 K, plotted in Figure 8, which reveal a monotonic increase up to the highest field without reaching saturation. For $0 \leq H_o \leq 80$ kOe, the high-field susceptibility obtained from the slope of the plot, χ_{HF} = 0.41 emu mol^{-1} kOe^{-1}; for $80 < H_o < 130$ kOe, χ_{HF} = 0.91 emu mol^{-1} kOe^{-1}; and for $140 < H_o < 230$ kOe, χ_{HF} = 0.12 emu mol^{-1} kOe^{-1}. There is no hysteresis in the magnetization and no remanent moment when the field is swept up to 230 kOe and back down to zero. At 230 kOe the moment (μ) per Fe_{11} aggregate approaches 17 μ_B. If we write eq 6, where $\langle S \rangle$ is the average spin per aggregate, the observed moment gives $\langle S \rangle = {}^{17}/_2$, for $g = 2$. For a pure $S_T =$

$$\mu = g\mu_B\langle S \rangle \quad (6)$$

${}^1/_2$ state, the ground state obtained by extrapolation from the temperature-dependent study (Figure 7), the magnetization would saturate at 1 μ_B per aggregate. The theoretical maximum, or full, magnetization corresponding to parallel alignment of all eleven $S = {}^5/_2$ ferric spins is 55 μ_B per aggregate. Thus, the moment

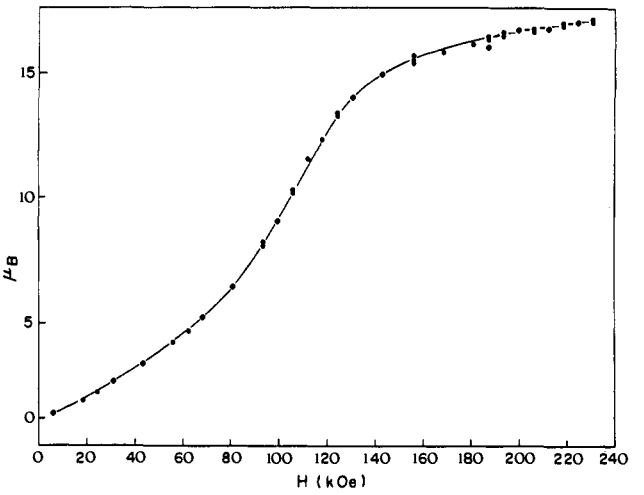

Figure 8. Magnetization studies of **1** at 1.3 K in which the magnetic moment per aggregate of **1** is plotted as a function of the field.

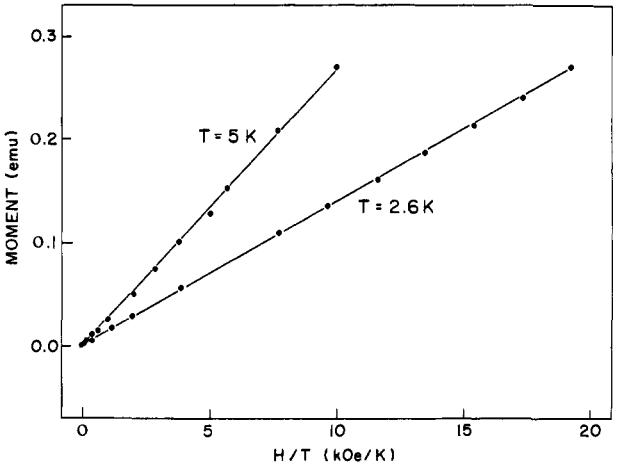

Figure 9. Magnetic moment per aggregate of **1** vs. H/T at 5.0 and 2.6 K.

at 230 kOe is approximately 33% of the value expected for full magnetization.

These data reveal that the Fe_{11} aggregate is not behaving as a simple paramagnet. Further evidence in support of this conclusion comes from plots of the magnetization as a function of H/T at 2 and 5 K (Figure 9), which otherwise would be congruent. The results can be explained on the basis of antiferromagnetic spin exchange within the undecairon(III) aggregates, however. Exchange coupling constants (J) for iron(III) centers linked by μ-oxo bridges are typically ca. −100 cm^{-1}, but protonation or metalation of the bridging oxygen atom can reduce the exchange interaction such that J = ca. −10 cm^{-1} [16,31,37] Both kinds of interactions occur in the undecairon(III) aggregate **1**. The stronger exchange interactions can be invoked to explain the fact that, at room temperature, the effective magnetic moment of 4.2 μ_B per iron is less than the value of 5.9 μ_B expected for uncoupled high spin ferric centers; they also account for the decline in μ_{eff} below ~100 K. The Zeeman energy level splitting of a spin with g = 2 in a magnetic field of 100 kOe is about 10 cm^{-1}. Thus the "step" in the magnetization between 100 and 140 kOe (Figure 8), which is reminiscent of a metamagnetic transition in magnetically ordered materials,[38] might correspond to the competition of the field with exchange energies typical of μ-hydroxo bridges.

Zero-field Mössbauer spectra are shown in Figure 10. The spectra consist of an asymmetrically broadened quadrupole doublet. The asymmetry reverses at about 80 K. The 80 K

(37) Armstrong, W. H.; Lippard, S. J. *J. Am. Chem. Soc.* **1984**, *106*, 4632–4633.
(38) Chikazumi, S. *Physics of Magnetism*; Wiley: New York, 1964; p 11.

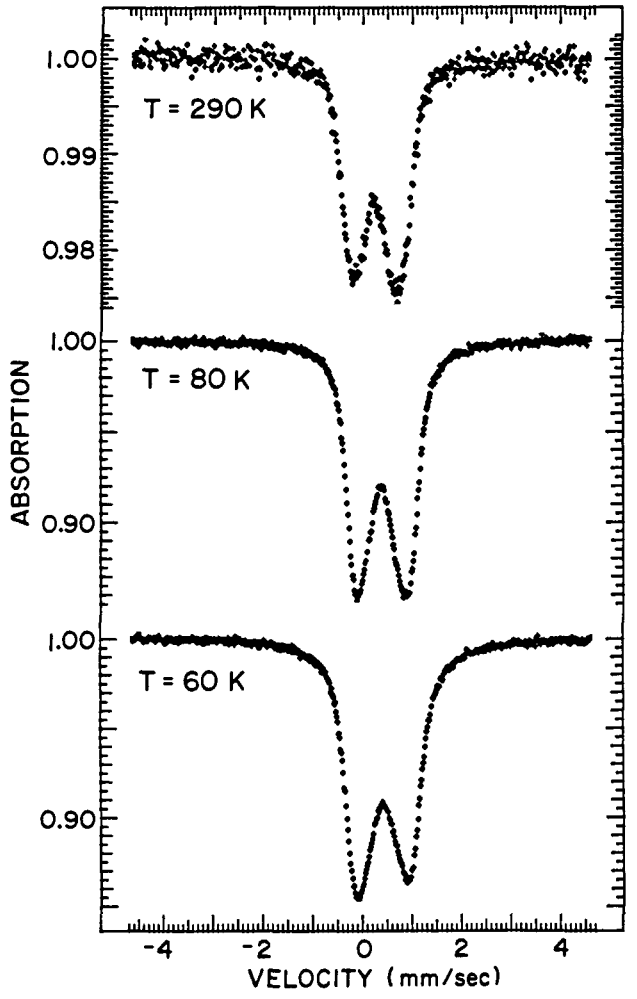

Figure 10. Zero-field Mössbauer spectra of **1** at three temperatures.

spectrum can be fit as a single broad quadrupole doublet with isomer shift (relative to iron metal at room temperature) $\delta = 0.50$ mm/s and quadrupole splitting $\Delta E = 0.91$ mm/s. These parameters are comparable to those in oxo-bridged high-spin ferric complexes.[39] The spectrum was also fit with three quadrupole doublets corresponding to the three crystallographically inequivalent iron sites A, B, and C with relative occupations 2:3:6. The fit was made with all parameters left free except for spectral areas, giving the results in Table V.

At 4.2 K, the zero-field spectrum is significantly broadened (Figure 11) with wings that extend from about +7 to −7 mm/s. Essentially the same spectrum is obtained at 2 K. The 5-kOe spectrum at 4.2 K is also similar to the zero-field spectrum, except for slightly more definition in the wings of the spectrum and asymmetry at the center (Figure 11). Above 30 kOe, there are six well-defined but broad lines superimposed on a broad background. Between 30 and 80 kOe, the line intensities increase relative to the unresolved background, but the line positions do not change appreciably. At 80 kOe, shoulders are discernible on the highest and lowest velocity lines.

The six lines in the 30-, 60-, and 80-kOe spectra correspond to the four $\Delta m = \pm 1$ and two $\Delta m = 0$ lines of a magnetic hyperfine spectrum with an average field at the nucleus of 430 kOe. If the hyperfine field were collinear with the applied field, the $\Delta m = 0$ line intensities would tend to zero and the overall splitting of the spectrum would change with increasing applied field, because the field at the nucleus is the vector sum of the applied field and the internal magnetic hyperfine field. The fact that the line centroids are relatively invariant and the $\Delta m = 0$ lines so intense

(39) (a) Greenwood, N. N.; Gibb, T. C., *Mössbauer Spectroscopy*; Chapman and Hall, Ltd.: London, 1971; pp 148–164. (b) Blume, M. *Phys. Rev. Lett.* **1967**, *18*, 305–307.

Table V. Selected Mössbauer Parameters for $[Fe_{11}O_6(OH)_6(O_2CPh)_{15}]$ and Related Polyiron Aggregates

material	T (K)	δ^a (mm/s)	$\Delta E_Q{}^b$ (mm/s)	H_{hf} (kOe)[c]	ref
$Fe_{11}O_6(OH)_6(O_2CPh)_{15}$	80	0.53	0.49		*d*
(**1**)		0.46	0.87		
		0.51	1.10		
	4.2			430	*d*
mammalian	100	0.45	0.72		*e*
ferritin	4.2			500	
A. vinlandii	80	0.48	0.78		*f*
ferritin	4.2			490	
E. coli	1.8			430	*g*
ferritin					
M. intermedia	4.2			420	*h*
dermal granules					
ferrihydrite	4.2			490	*i*
natural ferric	77		0.81		*j*
gel	4.2			460	

[a] Isomer shift with respect to iron metal at room temperature. [b] Quadrupole splitting. [c] Saturation hyperfine magnetic field. [d] This work. [e] Reference 46. [f] Reference 50. [g] Bauminger, E. R.; Cohen, S. G.; Dickson, D. P. E.; Levy, A.; Ofer, S.; Yariv, J. *Biochim. Biophys. Acta* **1980**, *623*, 237–242. [h] Ofer, S.; Papaefthymiou, G. C.; Frankel, R. B.; Lowenstam, H. *Biochim. Biophys. Acta* **1981**, *676*, 199–204. [i] Murad, E.; Schwertmann, U. *Am. Mineral.* **1980**, *65*, 1044–1049. [j] Reference 44.

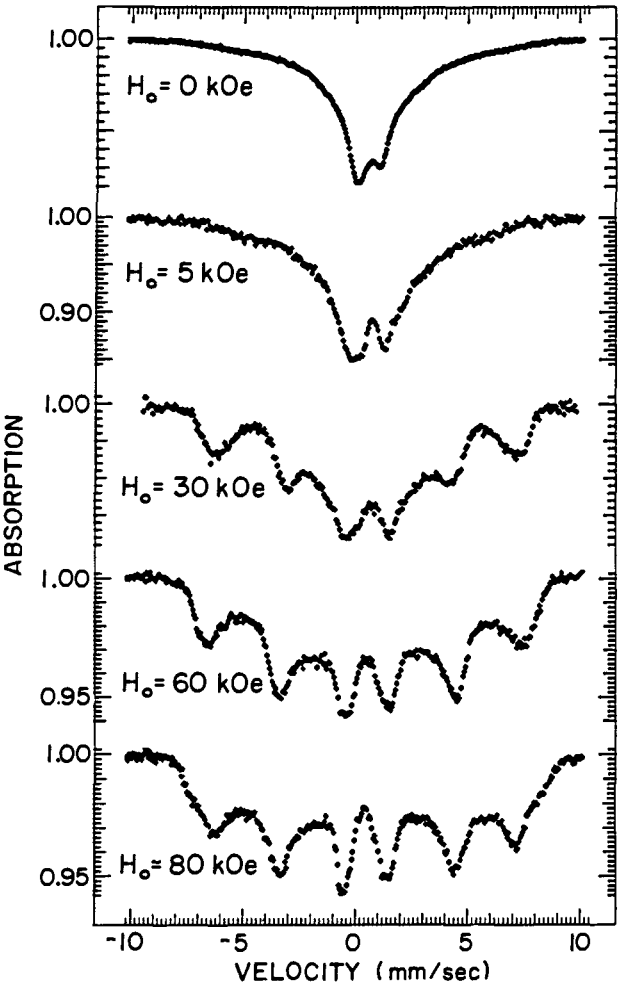

Figure 11. Field dependence of the Mössbauer spectrum of **1** at 4.2 K.

means that the magnetic hyperfine fields, and hence the local ferric ion magnetic moments, are preferentially oriented perpendicular to the applied field. Thus, increasing the applied field only marginally shifts the line positions. The broadening may be due to some inequivalency in the magnetic hyperfine fields for the different sites, as well as effects of averaging over the angle

between the magnetic hyperfine field and the principal component of the electric field gradient tensor. There is a measurable asymmetry in the splittings of the two highest velocity lines compared to the two lowest velocity lines, which is due to the quadrupole interaction.

In zero field, the net moment of the Fe_{11} aggregate does not have a fixed spatial orientation, but it relaxes with a certain frequency. At 4.2 K, the broadening of the Mössbauer spectrum implies that the relaxation time is of the order of the nuclear Larmor precession time, or about 10^{-7} s. Shorter relaxation times at higher temperatures obscure the magnetic hyperfine broadening.

The applied magnetic fields at low temperature will magnetize the net spin of the cluster along the field direction and decrease the relaxation time. Thus, magnetic hyperfine lines appear superimposed on the relaxation envelope in the Mössbauer spectrum and become more intense with increasing field. The magnetic hyperfine field of 430 kOe presumably corresponds to the full $S = {}^5/_2$ spin at each iron site in the aggregate. Although hyperfine fields of ~500 kOe occur for Fe^{3+} in magnetically ordered iron oxides such as Fe_2O_3,[40] fields ranging from 410 to 450 occur in some ferric oxyhydroxides (see Table V). The lower fields are probably associated with protonated or metalated bridging oxygens. From the intensity of the $\Delta m = 0$ lines, the Fe^{3+} spins are oriented more or less perpendicular to the applied field and hence to the net spin of the molecule. Since the extrapolated low-temperature moment ($g\mu_B S = 1\ \mu_B$ for $S = {}^1/_2$) is less than 2% of the theoretical full moment ($g\mu_B S = 55\ \mu_B$ for $S = {}^{55}/_2$), only a small canting of the spins from the perpendicular orientation is required to produce the net moment. Increasing the applied field causes the spins to tip toward the direction of the field, increasing the net moment. This model predicts that, in very high magnetic fields, the individual spins would eventually be oriented parallel to each other along the field direction, i.e., the moment of the cluster would approach 55 μ_B. The departure from linearity of the moment with applied field at about 100 kOe (Figure 8) suggests a transition to a new spin configuration in the aggregate. This new configuration may also be responsible for the appearance of the wings on the 80-kOe Mössbauer spectrum.

The magnetic properties of **1** may be compared with the superparamagnetism of small particles (<100 Å) of antiferromagnetically coupled ferric oxides and oxyhydroxides, such as ferrihydrite or the polyiron core of ferritin. These particles typically have a small net moment due to noncompensation of the two sublattices.[41] The sublattice magnetizations have a relaxation time τ which varies exponentially with temperature. For $T > T_B$, the so-called blocking temperature, the relaxation is rapid and the particles behave like a paramagnet, for example, the magnetization scales as H/T and there is no remanent magnetization. For $T < T_B$, the sublattices are essentially frozen, the magnetization is field dependent but essentially temperature independent, and there is a remanent magnetization. The blocking temperature varies from less than 4 to 30 K for ferritins from different sources.[42] The magnetic ordering, or Néel temperature, has been estimated to be ~200 K for mammalian ferritin.[43] A similar Néel temperature occurs in another natural ferric oxyhydroxide.[44] At room temperature, i.e., above the Néel temperature, the effective moments per iron are on the order of 3.9 μ_B.[45] The Mössbauer spectrum for $T < T_B$ is a broadened six-line spectrum with splitting that varies with the source of the ferritin (Table V). For $T > T_B$, the spectrum is a quadrupole doublet. For intermediate temperatures, $T \sim T_B$, the doublet and sextet coexist.

From the magnetic and Mössbauer data, it is evident that the undecairon aggregate has magnetic properties distinctly different from those of superparamagnetic ferritin. Its properties, however, also differ from those of simpler spin-coupled paramagnetic aggregates, such as $[Fe_3O(TIEO)_2(O_2CPh_2)Cl_3]$.[16] The characteristic features include the following: (1) rapid change in the effective moment with temperature at low temperature; (2) strong field dependence of the magnetization even at high values of H/T, but with no remanent moment; and (3) perpendicular orientation of the individual iron spins relative to the net moment of the cluster. These properties are suggestive of a small antiferromagnetically coupled particle with very low anisotropy and some exchange interactions on the order of 10 cm^{-1}. Thus, the Fe_{11} molecules may be regarded as having incipient magnetic order, which raises the intriguing question of how large a cluster needs to be to exhibit the superparamagnetic behavior of small antiferromagnetically coupled particles, such as the ferritin core.

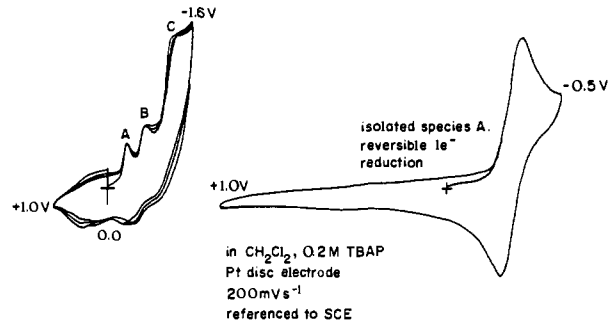

Figure 12. Cyclic voltammograms at 200 mV/s of **1** in CH_2Cl_2.

Redox Properties of $[Fe_{11}O_6(OH)_6(O_2CPh)_{15}]$. Figure 12 displays cyclic voltammograms of **1** dissolved in methylene chloride. Three reduction waves labeled A, B, and C appear between 0 and −1.6 V vs. the saturated calomel electrode. The cyclic voltammogram of species A is quasireversible with $E_{1/2}$ −0.309 V and a peak-to-peak potential (ΔE_{pp}) of 120 mV. The reversible ferrocene/ferricinium redox couple had a ΔE_{pp} of 110 mV under the same conditions. These results suggest that the undecairon(III) aggregate can be reduced to form $[Fe_{11}O_6(OH)_6(O_2CPh)_{15}]^-$, although overlap of this wave with that of species B made it impossible to confirm this assignment by controlled potential coulometry. Further reduction to form species B and C leads to decomposition, judging by the failure to observe clean anodic waves corresponding to their reoxidation upon reversal of the potential sweep in the cyclic voltammogram, as well as by the appearance of new electroactive species at positive potentials following several voltage cycles. The latter must derive from B and C, since they do not appear in the cyclic voltammogram of isolated species A (Figure 12). Addition of excess sodium benzoate to the solution produced no change in the scans. The electrochemical behavior of **1** is especially interesting in view of the fact that the loading and unloading of iron in the ferritin core is believed to involve Fe(II)/Fe(III) redox chemistry.[6] A reduction potential of ca. −0.20 V (vs. NHE) has been reported for the core of horse spleen ferritin in aqueous solution at pH 7.0,[46] compared to the value of −0.07 V (corrected vs. NHE) for **1** in CH_2Cl_2.

Possible Biological Relevance and Conclusions. A new discrete oxo-hydroxo-bridged polyiron aggregate has been synthesized. Its mode of formation, starting from simple iron salts and biologically relevant ligands, may be formally similar to the polymerization process that takes place during the formation of the metal core of the iron storage protein, ferritin. Formation of the undecairon aggregate is regulated by the amount of water present in the reaction mixture, the rate of water diffusion, and the presence of phenyl groups. The choice of the solvent and co-solvent is also important; two different crystalline forms of the same molecule were obtained when the reaction conditions were changed.

A bimetallic complex is formed between iron and apoferritin,[7,8] and this complex may represent the "matrix" onto which iron atoms subsequently add, resulting ultimately in formation of the

(40) van der Woude, F. *Phys. Status Solidi* **1966**, *17*, 417–432.
(41) Néel, L. *J. Phys. Soc. Jpn., Supple. 17, B1* **1962**, 676–684.
(42) St. Pierre, T. G.; Dickson, D. P. E.; Webb, J.; Kim, K. S.; Macey, D. J.; Mann, S. *Hyp. Int.* **1986**, *29*, 1427–1430.
(43) Blaise, A.; Chappert, J.; Giradet, J. L. *C. R. Acad. Sci. (Paris)* **1965**, *261*, 2310–2313.
(44) Coey, J. M. D.; Readman, P. W. *Earth Planet Sci. Lett.* **1973**, *21*, 45–51.
(45) Shoffa, C. *Z. Naturforsch.* **1965**, *20b*, 167–172.
(46) Watt, G. D.; Frankel, R. B.; Papaefthymiou, G. C. *Proc. Natl. Acad. Sci. U.S.A.* **1985**, *82*, 3640–3643.

polymer. In ferritin, the polymerization process could be regulated by access channels through the protein sheath and by phosphate anions. The latter are possible pH regulators. They may also serve to link crystallites that result during the polymerization process and act as counterions. The ratio of phosphate:iron may also be important in regulating the size of the crystallites. A higher number of phosphates results in smaller crystallites and a lower degree of crystallinity of the core.[6i,47-50]

In the formation of **1**, the phenyl rings may play the role of the protein sheath, but only up to its hydrophobic surface, with carboxylate groups anchored to it. A binuclear $\{Fe_2O\}^{4+}$ complex could bind to the carboxylate groups, forming Hr-like structures. Unlike Hr, the hollow apoferritin core allows subsequent addition of metal atoms to the initial complex, a possible first step in this direction being modeled by the $\{Fe_3O\}^{7+}$ and $\{Fe_4O_2\}^{8+}$ type complexes.[16-18] Slow addition of H_2O favors oligomerization as well as introduction of hydroxyl groups.

The structure of the $[Fe_{11}O_6(OH)_6(O_2CPh)_{15}]$ molecule reveals only octahedral coordination around iron, in agreement with the optical and near IR spectroscopy of ferritin; the magnetic and Mössbauer properties are also similar, but not identical. Preliminary electrochemical studies by cyclic voltammetry indicate that *the aggregate* can be reversibly reduced by one electron, compared with the one electron *per iron* reduction of mammalian ferritin.[46] The presence of THF or MeCN hydrogen bonded to the Fe_{11} core suggests a manner by which small molecules could facilitate the removal of iron from the ferritin core in accord with recent suggestions.[51,52] The phenyl rings form six rudimentary "channels" that may provide size and hydrophilic/hydrophobic selection for the "attacker", the same way that the ferritin protein sheath does.

Acknowledgment. This work was supported by National Institute of Health Research Grant GM 31234 (to S.J.L.) from the National Institute of General Medical Sciences. R.B.F. and G.C.P. were supported by the Office of Naval Research. The Francis Bitter National Magnet Laboratory is supported by the National Science Foundation. We thank R. L. Rardin and M. Hostettler for experimental assistance.

Supplementary Material Available: Tables of thermal parameters for all atoms, hydrogen positional and thermal parameters, and a full list of bond lengths and angles (18 pages); listing of observed and calculated structure factor amplitudes (74 pages). Ordering information is given on any current masthead page.

(47) Macara, I. G.; Hay, T. G.; Harrison, P. M. *Biochem. J.* **1972**, *126*, 151-162.
(48) Stiefel, E. I.; Watt, G. D. *Nature (London)* **1979**, *279*, 81-83.
(49) Mansour, A. N.; Thomson, C.; Theil, E. C.; Chasteen, N. D.; Sayers, D. E. *J. Biol. Chem.* **1985**, *260*, 7975-7979.
(50) Watt, G. D.; Frankel, R. B.; Papaefthymiou, G. C.; Spartalian, K.; Stiefel, E. I. *Biochemistry* **1986**, *25*, 4330-4336.
(51) Funk, F.; Lenders, J.-P.; Crichton, R. R.; Schneider, W. *Eur. J. Biochem.* **1985**, *152*, 167-172 and references cited therein.
(52) Jones, T.; Spencer, R.; Walsh, C. *Biochemistry* **1978**, *17*, 4011-4017.

Identification and Structural Implications of the 90 K Superconducting Phase†

H. Steinfink,* J. S. Swinnea, Z. T. Sui,‡ H. M. Hsu, and J. B. Goodenough

Contribution from the Center for Materials Science and Engineering, The University of Texas at Austin, Austin, Texas 78712. *Received March 30, 1987*

Abstract: The phase relations of Cu-containing compounds in the system Y_2O_3-BaO-CuO were determined at a temperature of about 950 °C and a fixed partial pressure of 0.21 atm of oxygen. Mixtures of Y_2O_3, $BaCO_3$, and CuO were heated and the products identified by powder X-ray diffraction. The stable ternary phases containing Cu are $Y_2Cu_2O_5$, Y_2BaCuO_5, $YBa_2Cu_3O_{8-y}$, and $BaCuO_2$. The 90 K superconducting material is $YBa_2Cu_3O_{8-y}$. It is an ordered phase and does not display detectable solid solution between Y and Ba. It is orthorhombic a = 3.824 (1) Å, b = 3.891 (1) Å, c = 11.685 (2) Å. A pseudotetragonal structure based on $a \approx b \approx 3.87$ Å, c = 11.68 Å, $P4/mmm$ has Y situated between square coplanar CuO_2 layers; there are no oxygen atoms at this level. In the stoichiometry $YBa_2Cu_3O_8$ the copper between Ba layers occupies a tetragonally distorted octahedron (c/a = 0.88). It is most likely that the oxygen vacancies are associated with this Cu-O octahedral layer in $YBa_2Cu_3O_{8-y}$. The dramatic increase in superconducting transition temperature on going from the K_2NiF_4 structure of $La_{2-x}Ba_xCuO_{4-y}$ to the $YBa_2Cu_3O_{8-y}$ structure is considered with reference to large bipolarons, the position of the d_{z^2} energy level relative to the Fermi energy, and the overlap of the Cu:3d and O:2p bands.

Following the initial report of Bednorz and Müller[1] of evidence for high-temperature (T_c > 30 K) superconductivity in a La-Ba-Cu-O mixed-phase system, numerous workers[2-4] identified the superconducting phase as $La_{2-x}M_xCuO_{4-y}$ (M = Ba, Sr, or Ca) having the tetragonal K_2NiF_4 structure. Although the initial work was stimulated by an earlier paper[5] on the oxygen-defect perovskites $La_{3-x}Ln_xBa_3[Cu^{II}_{5-2y}Cu^{III}_{1+2y}]O_{14+y}$, primary theoretical attention has been focused on phases based on the K_2NiF_4 structure.

For a variety of reasons, several groups have substituted yttrium for lanthanum in an attempt to make $Y_{2-x}M_xCuO_{4-y}$ analogues; these efforts resulted in a multiphase product in which an unidentified phase gave a superconducting transition temperature

† The Experimental and Results sections were presented at the American Crystallographic Association Meeting, March 16, 1987 in Austin, Texas.
‡ Northeast University of Technology Shenyang, People's Republic of China, Visiting Scientist.

(1) Bednorz, J. G.; Müller, K. A. *Z. Phys.* **1986**, *B64*, 189.
(2) (a) Takagi, H.; Uchida, S.; Katazawa, K., Tanaka, S. *Jpn. J. Appl. Phys. Lett.* **1987**, *26*, L123. (b) Uchida, S.; Takagi, H.; Tanaka, S.; Katazawa, K. *Jpn. J. Appl. Phys. Lett.*, in press. (c) Cava, R. J.; van Dover, R. B.; Battlog, B.; Rietman, E. A. *Phys. Rev. Lett.* **1987**, *58*, 408.
(3) Tarascon, J. M.; Greene, L. H.; McKinnon, W. R.; Hall, G. W.; Geballe, T. H. *Science* **1987**, *235*, 1373.
(4) Jorgensen, J. D.; Schuttler, H.-B.; Hinks, D. G.; Capone, D. W.; Zhang, K.; Brodsky, M. B.; Scalapino, D. J. *Phys. Rev. Lett.* **1987**, *58*, 1024.
(5) Er-Rakho, L.; Michel, C.; Provost, J.; Raveau, B. *J. Solid State Chem.* **1981**, *37*, 151.

0002-7863/87/1509-3348$01.50/0 © 1987 American Chemical Society